Petroleum Science 21 (2024) 2240–2256

Contents lists available at ScienceDirect

Petroleum Science

journal homepage: www.keaipublishing.com/en/journals/petroleum-science

Original Paper

# Reactive transport modeling constraints on the complex genesis of a lacustrine dolomite reservoir: A case from the Eocene Qaidam Basin, China

Ying Xiong [a], Bo Liu [b], Xiu-Cheng Tan [c, *], Zheng-Meng Hou [d], Jia-Shun Luo [d], Ya-Chen Xie [d], Kai-Bo Shi [a], Kun-Yu Wu [e]

[a] School of Earth and Space Sciences, Peking University, Beijing, 100871, China
[b] Institute of Oil and Gas, Peking University, Beijing, 100871, China
[c] China National Petroleum Corporation Key Laboratory of Carbonate Reservoirs, Southwest Petroleum University, Chengdu, 610500, Sichuan, China
[d] Institute of Subsurface Energy Systems, Clausthal University of Technology, Clausthal-Zellerfeld, Niedersachsen, 38678, Germany
[e] Research Institute of Exploration and Development, PetroChina Qinghai Oil Field Company, Dunhuang, 736202, Gansu, China

ARTICLE INFO

*Article history:*
Received 14 August 2023
Received in revised form
28 October 2023
Accepted 13 March 2024
Available online 14 March 2024

Edited by Jie Hao and Teng Zhu

*Keywords:*
Reactive transport modeling
Lacustrine dolomite
Mineralogy and porosity evolution
Reservoir genesis

ABSTRACT

Reactive transport modeling (RTM) is an emerging method used to address geological issues in diagenesis research. However, the extrapolation of RTM results to practical reservoir prediction is not sufficiently understood. This paper presents a case study of the Eocene Qaidam Basin that combines RTM results with petrological and mineralogical evidence. The results show that the Eocene Xiaganchaigou Formation is characterized by mixed siliciclastic-carbonate-evaporite sedimentation in a semiclosed saline lacustrine environment. Periodic evaporation and salinization processes during the syngenetic-penecontemporaneous stage gave rise to the replacive genesis of dolomites and the cyclic enrichment of dolomite in the middle-upper parts of the meter-scale depositional sequences. The successive change in mineral paragenesis from terrigenous clastics to carbonates to evaporites was reconstructed using RTM simulations. Parametric uncertainty analyses further suggest that the evaporation intensity (brine salinity) and particle size of sediments (reactive surface area) were important rate-determining factors in the dolomitization, as shown by the relatively higher reaction rates under conditions of higher brine salinity and fine-grained sediments. Combining the simulation results with measured mineralogical and reservoir physical property data indicates that the preservation of original intergranular pores and the generation of porosity via replacive dolomitization were the major formation mechanisms of the distinctive lacustrine dolomite reservoirs (widespread submicron intercrystalline micropores) in the Eocene Qaidam Basin. The results confirm that RTM can be effectively used in geological studies, can provide a better general understanding of the dolomitizing fluid-rock interactions, and can shed light on the spatiotemporal evolution of mineralogy and porosity during dolomitization and the formation of lacustrine dolomite reservoirs.


## 1. Introduction

Reactive transport modeling (RTM) is an emerging method used to address subsurface issues related to the coupling of multiphase flow, solute transport, and chemical reaction processes in porous media (Budd and Park, 2018; Xiao et al., 2018; Yang et al., 2022a). Due to a wide range of applicability in spatial-temporal scale and flexible resolution, the RTM approach has been extensively used in hydrology, geology, engineering and environmental sciences (Whitaker and Smart, 2007; Kaufmann, 2016; Deng et al., 2022). From the perspective of petroleum geology, the RTM approach has the unique advantages of forward modeling and quantitatively assessing the diagenetic fluid-rock interactions and the reaction-induced porosity and permeability changes at both geological and production timescales (Xu et al., 2006; Whitaker and Xiao, 2010;

* Corresponding author.
*E-mail addresses:* xiongying511602@163.com (Y. Xiong), tanxiucheng70@163.com (X.-C. Tan).

https://doi.org/10.1016/j.petsci.2024.03.008

Xiong et al., 2023). In the last decade, RTM studies on the hydrogeochemical mechanisms of multiple dolomitization processes (including reflux, geothermal convection, and fracture-controlled hydrothermal models) have been frequently reported (Gabellone et al., 2016; Lu and Cantrell, 2016; Wei et al., 2017; Yang et al., 2022b) and lay the foundation for the early use of this method in dolomite problems. A series of simulation results for topics such as fluid flow patterns, mineral changes, and favorable conditions for dolomitization process have also been discussed based on both genetic models and practical cases (Al-Helal et al., 2012; Yang et al., 2022a). Nevertheless, to verify the effectiveness of this numerical approach in various geological settings and to better understand the mechanisms of dolomitizing fluid-rock interactions, further investigations, especially on lacustrine dolomitization process, are needed. The mutual verification between measured geological data (e.g., petrographic observations, mineralogical tests, and laboratory physical experiments) and simulation results is a critical issue in the field.

As a unique environment for dolomite formation, lacustrine basins are very sensitive to regional tectonic and climate changes, and their geochemical and hydrological conditions vary frequently (Last, 1990; Warren, 2000; Wanas and Sallam, 2016; Ye et al., 2016). The Qaidam Basin, which was greatly influenced by the surrounding mountains and the adjacent fluvial or deltaic depositional systems in the Eocene, developed lacustrine mixed siliciclastic-carbonate-evaporite sedimentation and heterogeneous dolomite distribution (Li et al., 2018; Xiong et al., 2021b). Previous work based on petrography and isotopic-elemental geochemistry has indicated an early replacive genesis of the dolomite in the Eocene Qaidam Basin and that the dolomite-rich intervals are favorable hydrocarbon reservoir rocks (Yuan et al., 2015; Wang et al., 2020). However, the complex lacustrine environment and mineral composition and the highly mixed sediments have made it difficult to precisely constrain the mineral-porosity evolution and the mechanism of dolomite enrichment. The hydrocarbon exploration in lacustrine dolomite was also limited by the uncertainty of dolomite reservoir genesis. Therefore, in addition to qualitative (or conceptual) analysis using conventional petrographic and mineralogical evidence, quantitative methods, such as numerical simulation (Whitaker et al., 2004), should also be integrated to better constrain the spatiotemporal distribution of fluid-rock reactions and the resulting mineralogy and porosity changes during the dolomitization process. This is important to precisely characterize the heterogeneous dolomite abundance and predict high-quality dolomite reservoir in complex lacustrine environments, such as the Eocene Qaidam Basin and elsewhere with similar dolomitization process.

Based on the integrated measured data (petrography, mineralogy and reservoir physical properties) and numerical simulations, the objectives of our study were to: (1) verify the validity of the RTM approach in a study of diagenesis; (2) reconstruct the dynamic mineralogy and porosity evolution during dolomitization and assess the potential controlling factors; and (3) reveal the formation mechanisms of dolomite reservoirs and their relative importance. The results serve not only an academic purpose in better understanding the dolomitizing fluid-rock interactions but also have important applications for hydrocarbon exploration in lacustrine dolomite reservoirs.

## 2. Geological setting

The Qaidam Basin, which is located in the northeastern Tibetan Plateau, is a large intermontane and petroliferous basin and has an average elevation of ca. 3000 m. It is bordered by the Altyn Mountains to the northwest, the Kunlun Mountains to the south, and the Qilian Mountains to the northeast (Fig. 1a). The tectonic processes of the Tethys-Himalayan area are directly tied to the formation and growth of the Qaidam Basin, and the Cenozoic sedimentation and tectonic deformation in the basin record the growth of the Tibetan Plateau since the India-Eurasia collision (An et al., 2001; Tapponnier et al., 2001; Yin et al., 2002; Bian et al., 2019). In particular, the stepwise rise and growth of the Tibetan Plateau and the resulting regional climate change, including the uplift of surrounding mountains, the increasingly dry and cold climate, and the gradual closure of the hydrogeological environment, significantly influenced the paleotectonics and paleoenvironment in the Qaidam Basin (Fig. 1b; Fang et al., 2007; Yang et al., 2016; Ye et al., 2020). The Paleogene Qaidam Basin was characterized by a restricted-evaporative lacustrine environment (Fig. 1c) and a series of saline phenomenon, as indicated by the formation of widespread evaporites and red beds (Ye et al., 2016; Guo et al., 2017; Xiong et al., 2021b).

Although the Qaidam Basin experienced a secular drying trend during the Paleogene, alternating humid-arid conditions and short-term moisture shifts (the Asian interior doubthouse climate), which have been revealed to be linked to the 41-kyr obliquity cyclic mechanism (Abels et al., 2011; Bosboom et al., 2014), have also been documented preceding the Eocene-Oligocene Transition (EOT) (Fig. 1b). The western Qaidam Basin is located at the junction of the Altyn Mountains and the East Kunlun Mountains (Fig. 1c), and is very sensitive to the intermittent inputs of terrigenous materials and riverine freshwater during relatively humid climatic periods. Moreover, the studied Eocene Xiaganchaigou Formation in the western Qaidam Basin is characterized by high-frequency climate-driven depositional sequences that comprise a mixture of terrigenous clastics and clays, carbonates, and evaporites (Jiang et al., 2019; Wang et al., 2020). The carbonate intervals, especially those that are dolomite rich, are important reservoir rocks and further constitute multisets of source-reservoir-cap rock assemblages together with the interbedded organic-rich silty mudstone and low-permeability evaporites (mostly anhydrite rock), forming the favorable target for tight oil exploration in the western Qaidam Basin (Huang et al., 2017; Liu et al., 2017).

## 3. Materials and methods

### 3.1. Petrographic observation

To reveal the macro- and micro-characteristics of the lacustrine dolomites in the Eocene Qaidam Basin, petrographic observations were conducted first on a total of ca. 1200 m of core and 200 sections (using an optical microscope) from 25 boreholes that penetrated the Eocene Xiaganchaigou Formation. The rock structure, depositional sequence and vertical distribution of dolomite-bearing intervals were carefully documented. Based on core and thin section observations, 15 representative samples (see details in Supplementary Table S1) that contain abundant dolomite were then collected and prepared for further investigation of micrometer-scale petrography (e.g., size, morphology and alignment of dolomite crystals) using a field emission scanning electron microscope (FSEM). Particularly, 2 FSEM samples were polished via argon ion beam using the Hitachi IM4000 milling system and then sputter-coated with Au using the Hitachi MC1000 vacuum sputter coater to clearly show the size, microstructure and distribution of those sub-micron pores in dolomite layers. Observation of the FSEM samples was conducted at the Key Lab of Reservoir Description of CNPC, Lanzhou, using a Quanta 450 FSEM microscope with 20 kV of accelerating voltage under high vacuum.

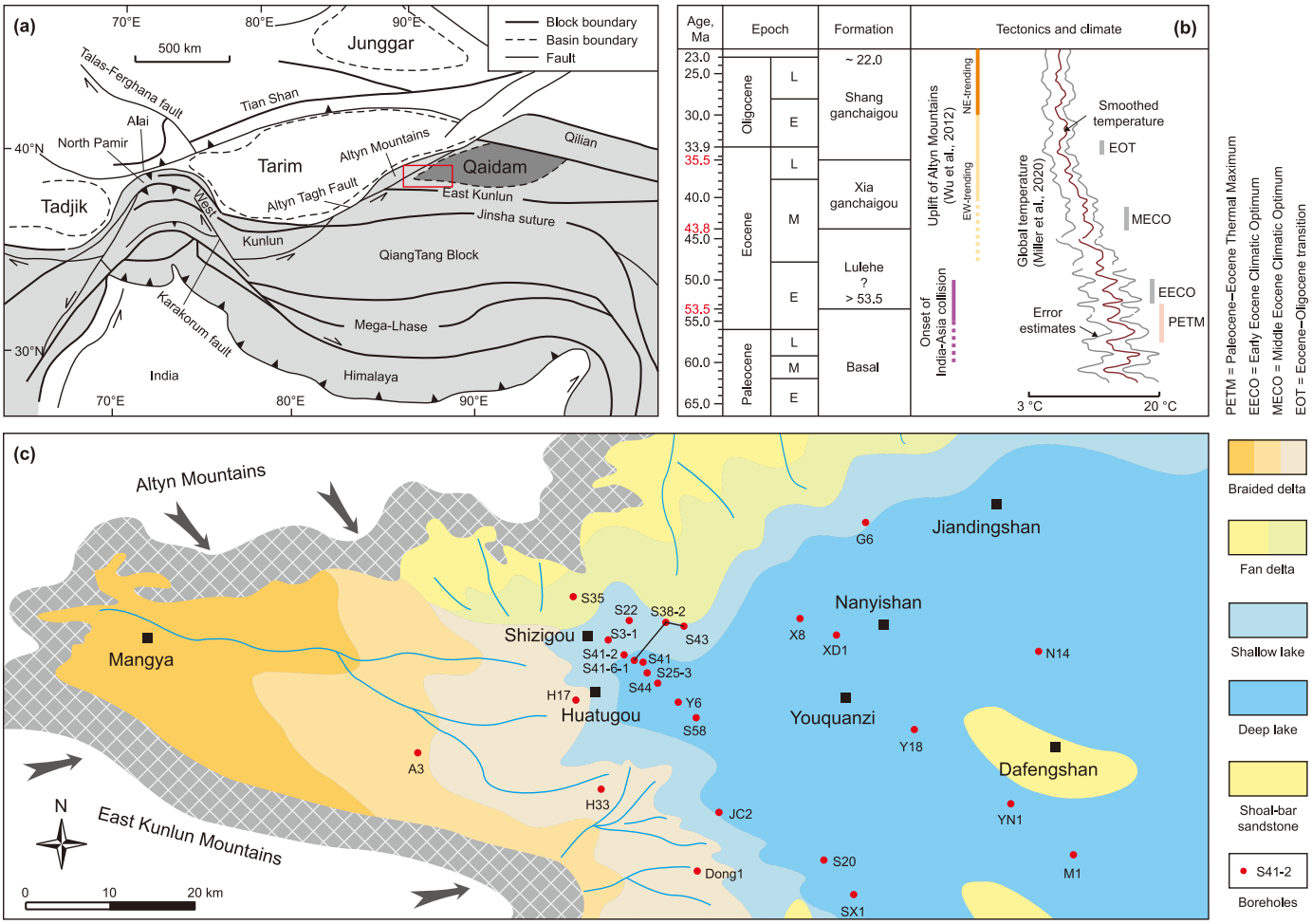


**Fig. 1.** Geological setting of the western Qaidam Basin (modified after Xiong et al., 2021b). (**a**) Schematic and tectonic map of Central Asia (modified after Sobel, 1999) showing the extent of the Tibetan Plateau (light gray), the locations of the Qaidam Basin (dark gray) and the study area (red rectangle). (**b**) Generalized stratigraphic column of the Paleogene Qaidam Basin showing the age framework (Bao et al., 2017), regional tectonics (Wu et al., 2012), and mean global temperature (Miller et al., 2020). **(c)** Paleogeographic map of the western Qaidam Basin during deposition of the Eocene Xiaganchaigou Formation (modified after Huang et al., 2017). The location is marked with red rectangle in (a).

### 3.2. Whole-rock X-ray diffraction

To determine the precise mineral composition of the lacustrine deposits and its variation with depositional sequences, a total of 223 samples were continuously collected from the high-quality core intervals of three boreholes (Wells 38-2, S41-6-1, and S43) for whole-rock X-ray diffraction (XRD) analysis. The whole-rock samples were first powdered using a rock grinding machine until the powders were finer than 200 mesh (<75 μm). Then, the crushed rock powders were collected and compressed into specimens for XRD analysis with an Empyrean diffractometer using mono-chromatic Cu, Kα radiation. Pretreatment of the samples and the analytical procedures were conducted at the Laboratory Center, Exploration and Development Institute of PetroChina Qinghai Oil Field Company. Identification of mineral types and calculation of relative contents were based on the diffraction patterns and peak intensity, following the procedures of the national standard "Analysis method for clay minerals and ordinary non-clay minerals in sedimentary rocks by the X-ray diffraction" (Chinese Standard SY/T 5163-2000).

### 3.3. Reactive transport modeling

In this research, the dolomitization process was simulated using the computer program TOUGHREACT (Xu et al., 2004), which was created by adding a reactive geochemistry module and linking thermo-hydro-chemical processes to the multiphase fluid and heat flow algorithm TOUGH2. This code has been successfully employed to simulate various diagenetic processes including dolomitization, karstification, dissolution-precipitation equilibrium of pore fluids, and hydrological circulation (Whitaker and Xiao, 2010; Garcia-Fresca et al., 2012; Yang et al., 2017; Xiong et al., 2021a).

Consistent with earlier RTM models of reflux dolomitization triggered by evaporated saline water (Jones and Xiao, 2005; Gabellone and Whitaker, 2016), changes in three mineral kinds (i.e., dolomite, calcite, and the concomitant gypsum/anhydrite) are considered in the dolomitization process. Calcite and gypsum dissolution and precipitation are modeled as thermodynamic processes that are governed by the pore fluid's saturation level and the fluid-rock system equilibrates (Whitaker and Xiao, 2010). Contrarily, dolomite precipitation is typically treated as a kinetic process and can be described through the general kinetic reaction rate law, which is compatible with the rate expression put forth by Lasaga et al. (1994):

$$r = k_d A_s \left(1 - \frac{Q}{K_{eq}}\right)^q \quad (1)$$

where $r$ [mol·s$^{-1}$] is the reaction rate, with positive values indicating mineral dissolution and negative values indicating precipitation, and $k_d$ [mol·m$^{-2}$ s$^{-1}$] is the temperature-dependent rate constant that can be expressed with the Arrhenius function:

$$k_d = Ae^{\frac{-E_a}{RT}} \quad (2)$$

Hence, the reaction rate of dolomite precipitation $r_{dol}$ can be expressed by:

$$r_{dol} = A_s A e^{-\left(\frac{E_a}{RT}\right)}\left(1-\frac{Q}{K_{eq}}\right)^q \quad (3)$$

where the specific reactive surface area $A_s$ relies on the size and shape of the dolomite particle,

$A$ is the pre-exponential factor and is set as 11.2 mol cm$^{-2}$ s$^{-1}$ here for dolomite precipitation according to previous RTM simulations (Gabellone and Whitaker, 2016), $E_a$ is the activation energy ($1.335 \times 10^5$ J mol$^{-1}$), $R$ is the universal gas constant, $T$ is the temperature (in Kelvin), $Q$ is the activity quotient in the fluids, $K_{eq}$ is the equilibrium constant of dolomite, and an empirical value of 2.26 is used for the reaction order ($q$) according to the specific laboratory experiment of dolomite precipitation conducted by Arvidson and MacKenzie (1999). The above approach for modeling the replacive dolomitization process and explanation of the relevant parameters have also been reported by Jones and Xiao (2005), Whitaker and Xiao (2010) and Gabellone and Whitaker (2016).

The reaction formulas, contents and thermodynamic-kinetic data of the included minerals in dolomitization are shown in Table 1. Xu et al. (2004) and the references therein provide additional computational models and details of the thermo-hydro-chemical coupled processes and the reaction-induced porosity and permeability variations involved in simulation. EQ (3)/6 geochemical database (Wolery, 1992), which is integrated with TOUGHREACT, was used to obtain the thermodynamic/kinetic rate parameters for aqueous species and minerals.

## 4. Results

### 4.1. Mineralogy of the mixed siliciclastic-carbonate-evaporite deposits

Whole-rock X-ray diffraction analysis shows that the Eocene Xiaganchaigou Formation is characterized by intensively mixed deposits and a very complex mineral composition that mainly includes carbonates (calcite and dolomite), evaporites (anhydrite, glauberite, and halite), siliciclastics (quartz and plagioclase), clays (kaolinite, illite and chlorite), and occasional pyrite. The mineral compositions of different samples are plotted in a ternary diagram (Fig. 2) and listed in Table S1. Carbonates are more abundant than terrigenous clastics (including detritus and clays) and evaporites. Specifically, dolomite has a relatively wide range of contents from 0 to 72.8% (28.2% ± 15.1%; reported as the mean value ± 1σ standard deviation), and calcite has contents of 0–54.3% (18.2% ± 10.7%).

Although the mineral composition is diverse and complex, a clear vertical variation trend in the mineral content, which occurs with the cyclic meter-scale depositional sequences, can also be observed (Fig. 3). Specifically, these sequences are generally 5–10 m in thickness and consist of dominant argillaceous clastic rocks (siltstone and argillaceous siltstone; >50%) and very few carbonates or evaporites (commonly <35%) in the lower part. However, the middle-upper parts of the sequences have appreciably higher contents of carbonates (>50%) and less siliciclastics and clays (10–35%). Moreover, the dolomite content usually exhibits an upward-increasing trend. Evaporites (mostly anhydrite and glauberite) occur mainly in the upper or top parts of the sequences and are commonly in disconformable contact (erosion and dissolution surfaces can be found) with the overlying siliciclastics/clay-dominated rocks at the base of the next deposition sequence. In general, the studied interval is characterized by the vertical superposition of cyclic meter-scale depositional sequences, and the mineral paragenesis varies within a sequence (from bottom to top) from argillaceous clastics to carbonates, and then to sulfates and chloride.

### 4.2. Dolomite petrography

As mentioned above, dolomites are generally enriched in the middle-upper part of a depositional sequence and occur in association with diverse siliciclastic-carbonate-evaporite deposits. Core observation shows that dolomite-rich carbonate rocks commonly have a dark gray massive structure (dozens of cm; Fig. 4a) or exhibit a thin-bedded structure that comprises frequent alterations of dark gray dolomite and light gray siliciclastic layers (a few cm; Fig. 4b). A few macrocrystalline glauberite-anhydrite associations, which are mostly 5 mm–2 cm in individual size, can also be observed in the upper part of the dolomite-rich intervals (Fig. 4c). Under the optical microscope, dolomites have typical microcrystalline structures and some pyrite and siliciclastics are scattered in the rocks (Fig. 4d and e). In local areas, the dolomite-rich intervals contain typical microbial fabrics such as stromatolitic laminae and thrombolytic clot clusters (Fig. 4f). The crystal morphology and size of these microcrystalline dolomites can be further identified under the FSEM. The dolomite crystals, generally 2.5–10 μm in size, have relatively ideal crystalline morphologies that feature euhedral rhombohedral textures (Fig. 4g). Furthermore, abundant submicron (mostly hundreds of nm) intercrystalline micropores can be clearly observed in the FSEM samples polished with argon ion beams, displaying an irregular serrated pore morphology (Fig. 4h). Mineral dissolution can be found at the edge of some dolomite crystals (Fig. 4i), forming

**Table 1**
Mineral parameters used for simulation.

| Parameters | Values (Source) |
|---|---|
| Calcite reaction formula | $CaCO_3 + H^+ \rightleftharpoons Ca^{2+} + HCO_3^-$ |
| Dolomite reaction formula | $Mg^{2+} + Ca^{2+} + 2HCO_3^- \rightleftharpoons MgCa(CO_3)_2 + 2H^+$ |
| Gypsum reaction formula | $Ca^{2+} + SO_4^{2-} + 2H_2O \rightleftharpoons CaSO_4 \bullet 2H_2O$ |
| Anhydrite | Assumed to be formed during burial via gypsum dehydration |
| Siliciclastics, glauberite and halite | Assumed to be nonreactive during dolomitization process |
| Initial mineral combination | 5% dolomite; calcite, gypsum, and clastics vary with depth |
| Thermodynamics and kinetics | Thermodynamics for calcite and gypsum; kinetics for dolomite |
| Dolomite kinetic rate constant | $4.58e^{-19}$ mol m$^{-2}$ s$^{-1}$ (Gabellone and Whitaker, 2016) |
| Dolomite reactive surface area | 5000 cm$^2$ g$^{-1}$ for basecase; 2500 and 10,000 for sensitivity analysis |
| Dissociation constants ($lg(K_{25^\circ C})$) | Calcite: 1.849; Dolomite: 2.514; Gypsum: −4.482 (EQ (3)/6 database) |

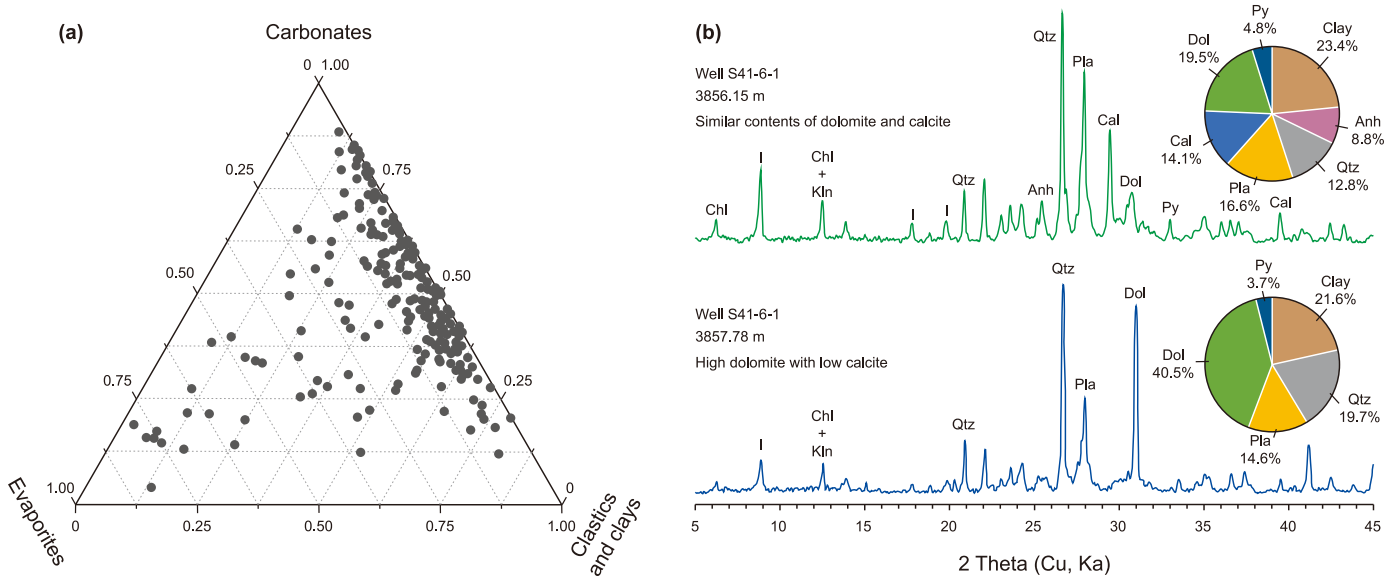


**Fig. 2.** Mineralogical composition of the Eocene Xiaganchaigou Formation in the western Qaidam Basin. (**a**) Ternary diagram showing the major mineral contents of the mixed siliciclastic-carbonate-evaporite deposits. (**b**) X-ray diffraction patterns of representative samples with different dolomite/calcite abundances (data from Xiong et al., 2021b). The relative contents of minerals are displayed in pie charts. The mineral peaks show: Qtz – quartz, Pla – plagioclase, Cal – calcite, Dol – dolomite, Py – pyrite, Anh – anhydrite, I – illite, Chl – chlorite and Kln – kaolinite.

dissolution etch pits and leading to a slight expansion of intercrystalline micropores.

### 4.3. Reactive transport modeling

#### 4.3.1. Model construction

(1) Grid system and rock properties

A simplified 1D grid system was used to simulate the dolomitization process, which depicts the replacement of calcite by dolomite from the near-surface to deeper strata (Fig. 5). The 10 m long column, which represents a common thickness of an individual depositional sequence in the study area, is evenly discretized into 40 grid cells. In response to the complex mineral compositions of the mixed carbonate-clastic-evaporite deposits in the lacustrine basin, four types of initial mineral (i.e., calcite, dolomite, clastics, and gypsum) are included in the grid system. The contents of initial mineral also vary with vertical burial depth (Fig. 5), representing the successive change in mineral paragenesis from clastics rocks to carbonates to evaporites within an upward-shallowing depositional sequence. To be specific, the calcite and gypsum display an increasing trend from the bottom to the top of the column, with the contents changing from 5% to 55% (whole-rock volume fraction) and from 4% to 14%, respectively. The contents of clastic mineral (including clays), however, decrease from 76% at the bottom to 16% at the top. In addition, an initial 5% "seed" dolomite (Gabellone and Whitaker, 2016) is involved to provide primary nucleation sites for dolomite precipitation, and an initial 10% rock porosity is specified throughout the column.

In the previous RTM studies of near-surface dolomitization (Jones and Xiao, 2005; Al-Helal et al., 2012), the initial porosity and permeability of grid cells were traditionally specified as the depositional porosity-permeability determined by the petrophysical relationships of the carbonate rock-fabric proposed by Lucia (1995), thus yielding a relatively high initial porosity of 30%–40%. However, the stratum we studied here is characterized by complex and mixed carbonate-clastic-evaporite deposits that should be considerably different from the pure carbonate sediments of previous studies. Given the dominant fine-grained sediments (micritic limestone and argillaceous siltstone) and the non-negligible terrigenous clays (with contents of 5%–30%) in the lacustrine environment, we specified a relatively low initial porosity of 10% and permeability of $3.85 \times 10^{-12}$ $m^2$ throughout the column. Reactive surface area (RSA) is another important parameter for simulating dolomitization process because it controls directly the reaction rate of kinetic minerals (Gabellone and Whitaker, 2016). Although there is currently no convincing data of the precise RSA of complex geological porous media, the particle size and morphology of the minerals can be used to approximate the RSA (German and Park, 2009). In this study, the RSA of dolomite is assumed to be 5000 $cm^2$ $g^{-1}$ for the base case scenario, indicating the 5 μm-diameter dolomite rhomb. Given the variable dolomite crystal size (2.5 μm–10 μm) as witnessed under the FSEM, two additional RSA values, i.e., 2500 $cm^2$ $g^{-1}$ and 10,000 $cm^2$ $g^{-1}$, were considered for sensitivity analysis, which are indicative of the 10 μm- and 2.5 μm-diameter dolomite rhombs, respectively.

(2) Hydrogeochemical conditions

Simulation of the dolomitization process was performed under a temperature condition of 26.2 °C that represents the average diagenetic temperature of dolomite in the study area as calculated by Yuan et al. (2015) using oxygen isotope thermometers. The chemical compositions of the initial and boundary water were derived from the present-day formation water chemistry in the study area measured by Huang et al. (2015). Notably, although the formation water does not directly reflect the syngenetic original/evaporated water chemistry since it is the final product of a series of water-rock reactions and concentration/dilution effects, under condition of a weak diagenetic alteration by burial fluids the formation water still preserves information such as the type and relative concentration of aqueous species. Hence, the measured formation water can be used as the foundation of the water chemistry associated with dolomitization. To be specific, the formation water, with a salinity of 22.6‰ in equilibrium with calcite

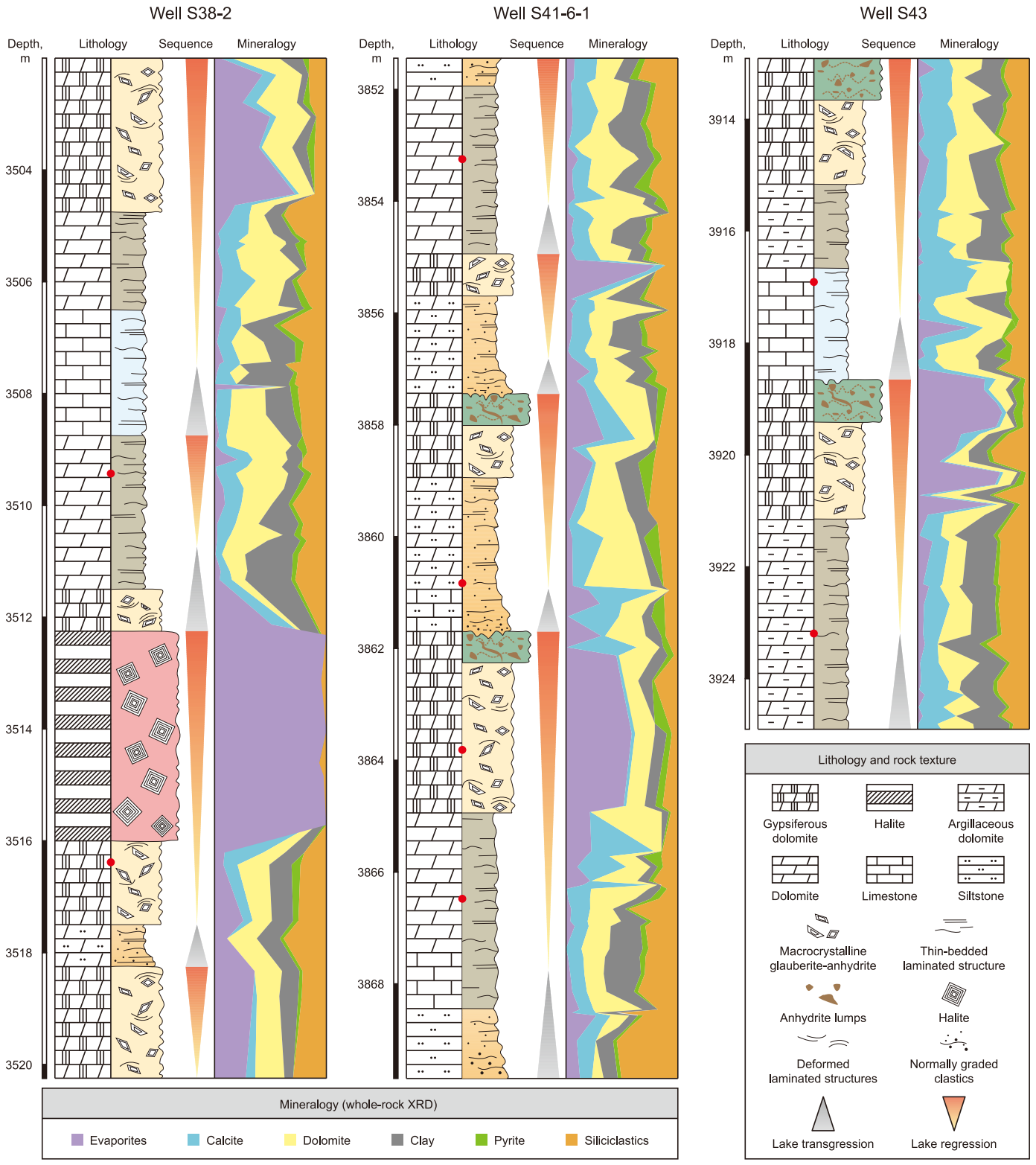


**Fig. 3.** Comprehensive lithological columns of the cored intervals of three boreholes showing the lithology, rock textures and mineral compositions with variation in depositional sequences in the Eocene Xiaganchaigou Formation. The red points mark the sample positions of petrographic observation. Locations of the boreholes are shown in Fig. 1c, marked with a cross-section (dark line).

and gypsum (calculated using the aqueous geochemical modeling code PHREEQC on the basis of its embedded thermodynamic database *PHREEQC. DAT*; Parkhurst and Appelo, 1999), was assumed to have originally saturated the grid system. The boundary water was generated by simulating evaporation of the formation water, and different salinities, i.e., 45.2‰, 113‰ (base case), and 226‰ were assessed to evaluate the impact of evaporation intensity on the dolomitization (Table 2). During simulation, the boundary

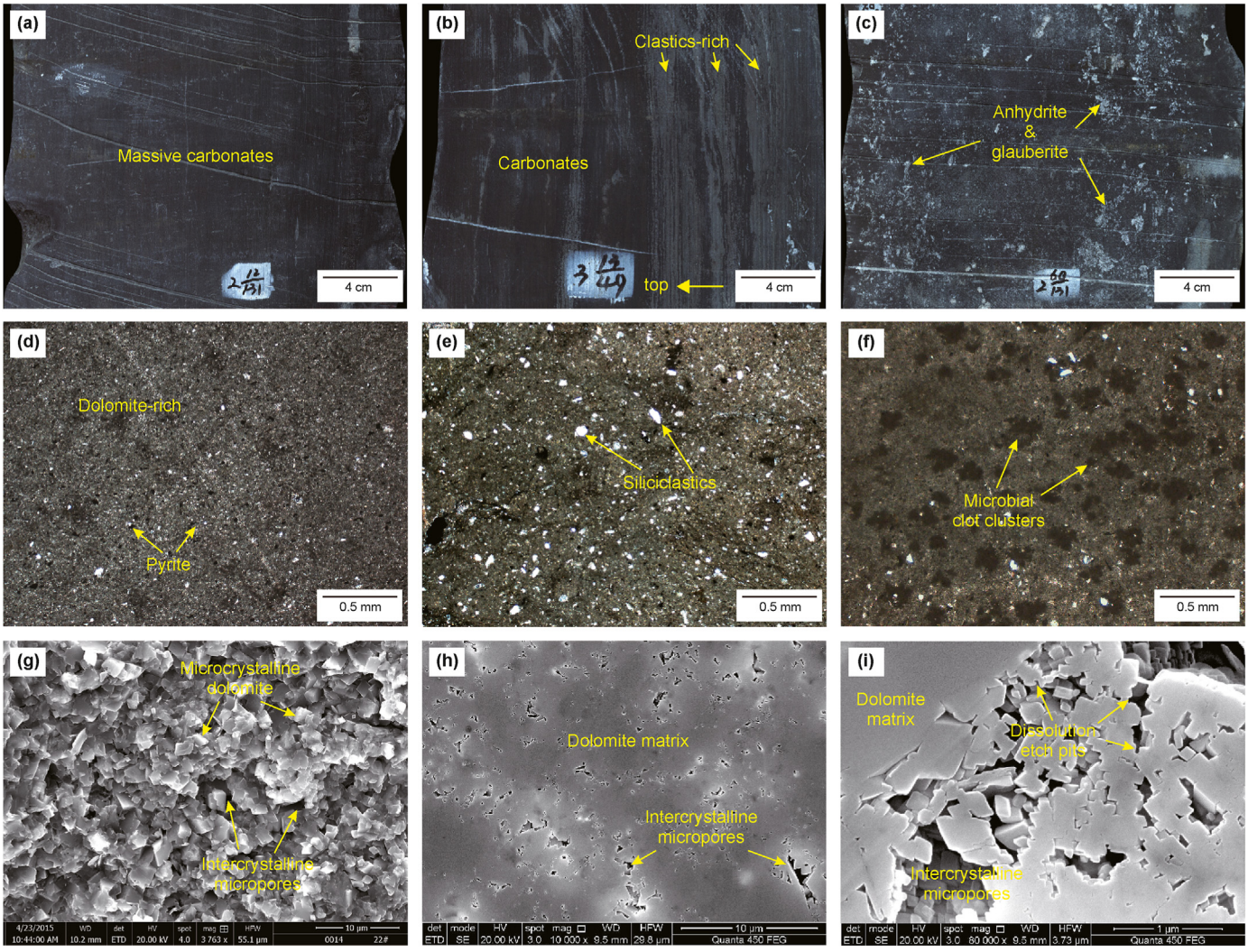


**Fig. 4.** Macro- and microscopic petrographic features of dolomite. (**a**) Dark gray massive dolomite-rich carbonate rocks. Well S41-2, 4075.4 m, core. (**b**) Thin-bedded structure that comprises frequent alterations of dark gray dolomite and light gray siliciclastic layers. Well 41-2, 4093.8 m, core. (**c**) Macrocrystalline glauberite-anhydrite crystals associated with dolomite-rich rocks. Well S41-2, 4081.0 m, core. (**d**) Microcrystalline dolomites and scattered pyrite. Well S41-2, 4162.6 m, thin section, cross-polarized light (CPL). (**e**) Microcrystalline dolomites and scattered siliciclastics. Well 41-2, 4176.1 m, CPL (Xiong et al., 2021b). (**f**) Thrombolytic clot clusters in dolomite-rich rocks, Well S41-6-1, 3853.7 m, CPL. (**g**) Euhedral rhombohedral dolomite microcrystals, Well S23, 4150.9 m, field emission scanning electron microscope (FSEM). (**h**) Sub-micron intercrystalline micropores in dolomite-rich rocks, Well S3-1, 4365.6 m, FSEM (argon ion beam polished). (**i**) Dissolution etch pits at the edge of dolomite microcrystals, Well S3-1, 4365.6 m, FSEM (argon ion beam polished).

water flows downwards from the top of the column (brine pond cell), representing the downward infiltration of evaporated lake water triggering the dolomitization. Table 3 lists the petrological and hydrogeochemical parameters used for simulations in different scenarios.

### 4.3.2. Model results

(1) Temporal and spatial distribution of minerals

The results of the base case simulation show the progressive dolomitization process from the top to the bottom of the column. In general, the change in the dolomite volume shows an increasing trend with simulation time but a decreasing trend with increasing depth and distance from the brine (evaporated water) source (Fig. 6a). During initial dolomitization (≤500 yr), dolomite precipitation can only be observed in a relatively shallow area (0 to −4.0 m). With time, the dolomitization tends to reach an equilibrium in the upper part of the column at a simulation time of approximately 1 kyr, yielding a maximum dolomite increase of 43.2% in the top grid cell. After 5 kyr, the evaporated water seeps throughout the column and gives rise to pervasive dolomitization that features a linearly upward-increasing change in the dolomite volume.

In response to dolomite precipitation, calcite decreases gradually with dolomitization (Fig. 6b). There is also a decreasing trend in calcite dissolution with increasing depth and distance from the brine source. Moreover, the vertical extent (depth) of calcite dissolution is the same as that of dolomite precipitation. At equilibrium (5 kyr), the amount of calcite dissolution reaches a maximum of −49.5% at the top of the column, with a downward-decreasing trend.

In comparison with dolomite and calcite, the change in the gypsum volume is complicated (Fig. 6c). In general, gypsum shows a dynamic evolution during dolomitization that is characterized by weak precipitation in the early stage followed by substantial

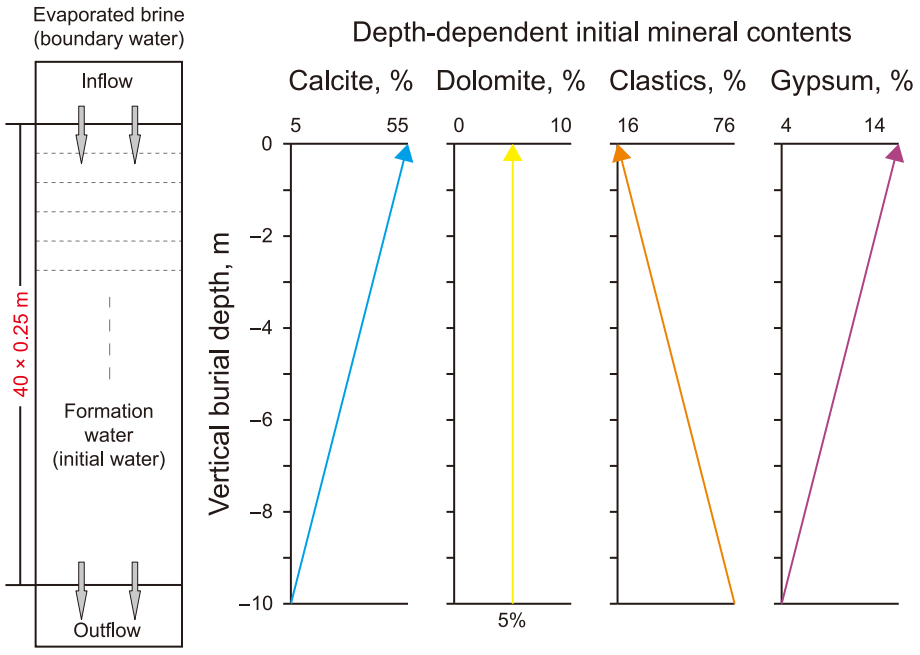


**Fig. 5.** Schematic illustration of the vertical column grid system and depth-dependent initial mineral composition.

**Table 2**
Chemical compositions of the different fluids used for simulation.

| Component, mol·L$^{-1}$ | Initial water | Boundary water I | Boundary water II | Boundary water III |
|---|---|---|---|---|
| $Na^+$ | $2.54e^{-1}$ | $5.27e^{-1}$ | $1.58e^{0}$ | $4.43e^{0}$ |
| $Cl^-$ | $3.98e^{-1}$ | $8.23e^{-1}$ | $2.47e^{0}$ | $6.94e^{0}$ |
| $K^+$ | $7.52e^{-2}$ | $1.56e^{-1}$ | $4.68e^{-1}$ | $1.30e^{0}$ |
| $Ca^{2+}$ | $5.76e^{-2}$ | $4.75e^{-2}$ | $1.43e^{-1}$ | $3.40e^{-1}$ |
| $Mg^{2+}$ | $3.50e^{-1}$ | $7.25e^{-1}$ | $2.19e^{0}$ | $6.11e^{0}$ |
| $HCO_3^-$ | $8.82e^{-4}$ | $1.63e^{-3}$ | $4.89e^{-3}$ | $1.37e^{-2}$ |
| $SO_4^{2-}$ | $4.17e^{-2}$ | $1.46e^{-2}$ | $4.08e^{-2}$ | $1.01e^{-1}$ |
| Salinity, ‰ | 22.6 | 45.2 | 113.0 | 226.0 |
| **Saturation Index** | | | | |
| Calcite | 0.00 | −0.62 | −0.27 | −0.66 |
| Dolomite | 0.94 | 0.15 | 1.00 | 0.57 |
| Gypsum | 0.00 | −0.73 | −0.03 | 0.84 |

**Table 3**
Petrological and hydrogeochemical parameters used for simulation.

| Parameters | Values (Source) |
|---|---|
| Initial porosity | 10% |
| Initial permeability | $3.85 \times 10^{-12}$ m$^2$ |
| Temperature | 26.2 °C (average diagenetic temperature of dolomite; Yuan et al., 2015) |
| Initial water | Normal lake water (salinity = 22.6‰; derived from Huang et al., 2015) |
| Boundary water | Evaporated lake water (salinity = 45.2‰, 113‰, and 226‰) |
| Fluid injection rate | 0.8 m yr$^{-1}$ |

dissolution in the late stage. For instance, the maximum amount of gypsum precipitation is 6.2% at a depth of −3.0 m after 2 kyr of simulation, while the upper part of the column (0 to −1.8 m) has a negative value of gypsum change. In the vertical direction, the location of gypsum precipitation is consistent with the dolomite front zone where the replacement reaction just reaches equilibrium. At equilibrium, the gypsum content tends to be lower than its initial value, and the maximum amount of gypsum dissolution is −12.6% at the top of the column.

(2) Porosity changes

The rock porosity displays a dynamic variation during dolomitization that is characterized by a slight decrease in the early stage followed by a significant increase in the late stage (Fig. 6d). Notably, during the early stage of dolomitization (≤1 kyr), the porosity shows a continuously increasing trend, and the process of porosity decrease was not observed. At a simulation time of 2 kyr, dynamic decrease/increase processes can be observed, and the depth range of porosity decrease corresponds to the gypsum precipitation interval. The maximum amount of porosity decrease is −1.6% at a depth of −3.0 m. After pervasive dolomitization, the rock porosities are apparently higher than their initial values, showing an upward-

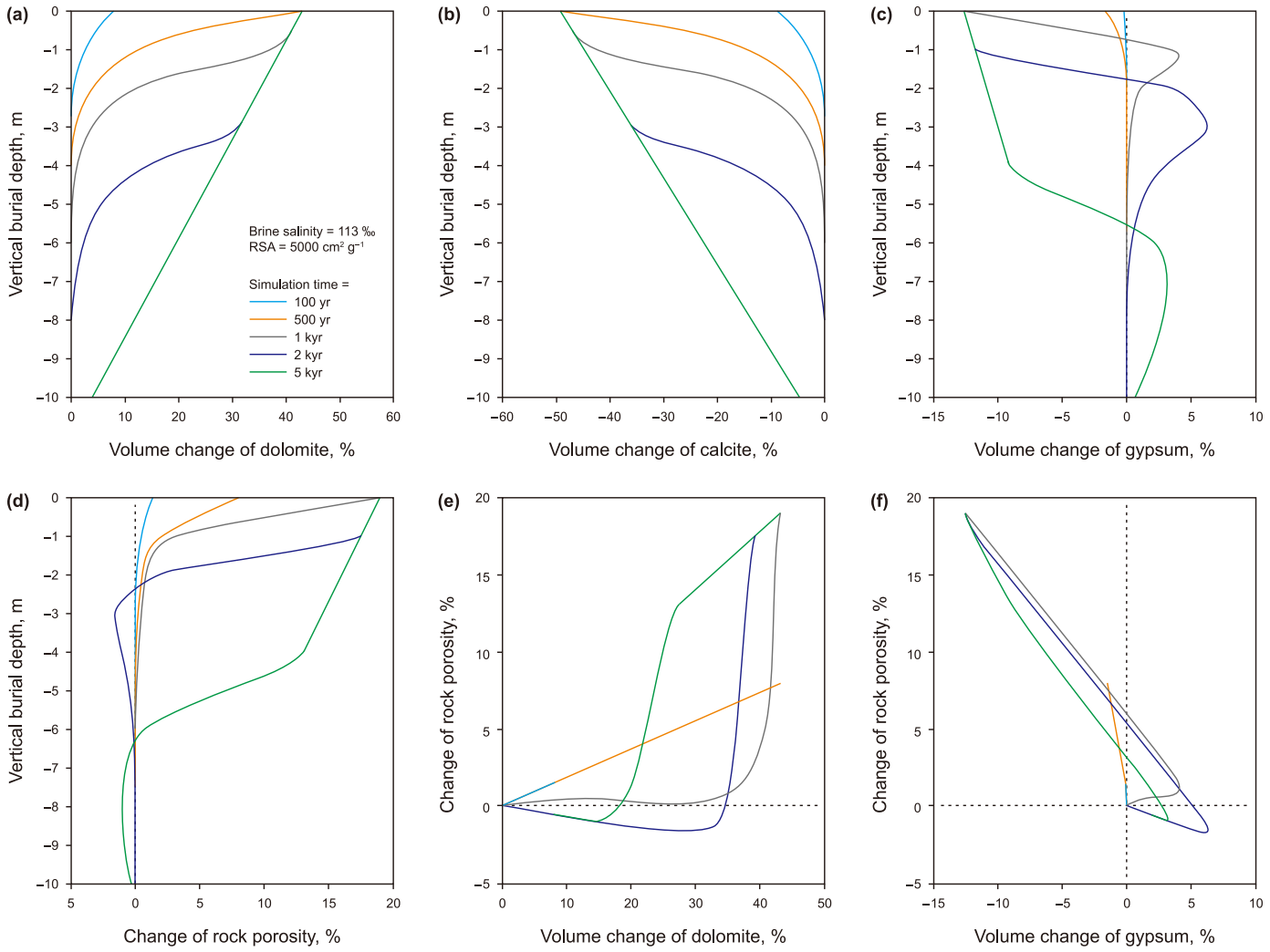


**Fig. 6.** Simulation results of the base case scenario showing the volume changes in (**a**) dolomite, (**b**) calcite, (**c**) gypsum, and (**d**) rock porosity with variation in simulation time and the relationships between (**e**) dolomite and (**f**) gypsum changes with rock porosity changes.

increasing trend in increased porosity that reaches a maximum of 18.9% at the top of the column.

Crossplots of rock porosity with dolomite and gypsum changes show a complex evolution of porosity during dolomitization (Fig. 6e and f). In general, two distinct patterns of porosity variation can be observed. For short periods of dolomitization ($\leq$1 kyr), the porosity increment shows a positive relationship with the dolomite increase, although there is a small amount of gypsum precipitation during this period. For longer periods of dolomitization (2–5 kyr), however, the rock porosity displays a dynamic decrease/increase process. Specifically, during the early stage of dolomitization with relatively low dolomite contents (ca. < 33%) and apparent gypsum precipitation, the rock porosity shows a slight decreasing trend. Subsequently, with increasing degrees of dolomitization and dissolution of gypsum (including early-precipitated gypsum cement and initial gypsum), the rock porosity increases dramatically.

## 5. Discussion

### 5.1. Dolomite genesis and variation in dolomite abundance

The petrogenesis of the microcrystalline dolomites in the western Qaidam Basin has been widely studied, and a replacive dolomitization model (driven by evaporation during the syngenetic-penecontemporaneous stage) is generally acknowledged (Yuan et al., 2015; Huang et al., 2016; Wang et al., 2020). Our results, which are based on petrographic and mineralogical analyses and RTM simulations, are comparable to previous findings, and further reveal the controls of periodic salinization processes on the occurrence of dolomitization and the vertical heterogeneity in dolomite abundance. First, the dolomites in the Eocene Qaidam Basin have a homogeneous very finely microcrystalline structure (Fig. 4d and e), which is highly similar to the petrological features (prior to burial recrystallization) of the products of large-scale early dolomitization in other evaporative lacustrine or marine environments (Feng et al., 1998; Machel, 2004), except that our dolomite samples show a higher contamination of detrital sediments due to the basin's paleogeographic position bounded by the Altyn Mountains and the East Kunlun Mountains. Second, other fabrics/textures, such as dolomite crystal overgrowth and mosaic structure, and saddle dolomite with associated hydrothermal minerals, which are indicative of burial dolomitization (recrystallization) and hydrothermal alteration, were not found in the study area. Furthermore, systematic X-ray diffraction analysis of the cored intervals show that the dolomite abundance co-varies with the high-

frequency meter-scale depositional sequences and usually reaches higher contents in the middle-upper part of an individual sequence (Fig. 3). This indicates that the occurrence of dolomitization and variation in dolomite abundance were likely linked to the multi-stage lake level fluctuations and salinization processes (Fig. 7).

To be specific, as demonstrated in previous studies, the Eocene Qaidam Basin featured a generally salinized lacustrine environment with periodic short-term variations in lake level and water salinity (Jiang et al., 2019; Xiong et al., 2021b). This setting was collectively controlled by the Asian interior doubthouse climate (driven by the 41-kyr obliquity cycle) preceding the EOT, which featured alternating humid-arid climate conditions and short-term moisture shifts superposed on a secular drying trend (Abels et al., 2011; Bosboom et al., 2014), and by the regional tectonic activity (i.e., uplift of the Altyn Mountains; Jolivet et al., 2001; Guo et al., 2018). For an individual depositional sequence, the early stage was characterized by rapid deposition during a lake transgression, corresponding to an intermittent humid climatic period. Abundant terrigenous materials and freshwater inputs from the adjacent fluvial deltaic depositional systems led to the relatively low salinity of the lake water and high contents of clastic and argillaceous sediments. As such, the lower part of the sequence is dominated by fresh-brackish water lacustrine deposits comprised dominantly of siltstone and argillaceous siltstone with a small quantity of carbonates (Fig. 7a and 8). With periodic climate change from humid to arid, the detrital-dominated deposition was gradually replaced by chemical deposition due to the decrease in the terrigenous supply. The lacustrine basin underwent a stage of brackish-saline water deposition during the early-middle lake regression, resulting in the dominance of carbonates (calcite) and a small quantity of sulfate (gypsum and glauberite), constituting the middle-upper part of the sequence (Fig. 8). Meanwhile, the strong evaporation during this period facilitated the formation and accumulation of high-salinity and high-density magnesium-rich brine (evaporated lake water) in the paleo-lowlands of the basin, which then triggered replacive dolomitization of the initially limestone sediments during downward infiltration (Fig. 7b). As a result, the dolomite content displays an upward increasing trend. During the late stage of lake regression, continuous evaporation resulted in a very high water salinity and low lake level, and the mineral paragenesis was transformed from carbonate to sulfate (gypsum and glauberite) and chloride (halite). Thus, the top part of sequence was dominated by hypersaline water deposits that comprise mostly evaporites with a dramatic decrease in the carbonate content (Fig. 8). Due to the fluctuating humid–arid climate conditions and water salinity variations, these processes were repeated, ultimately resulting in the

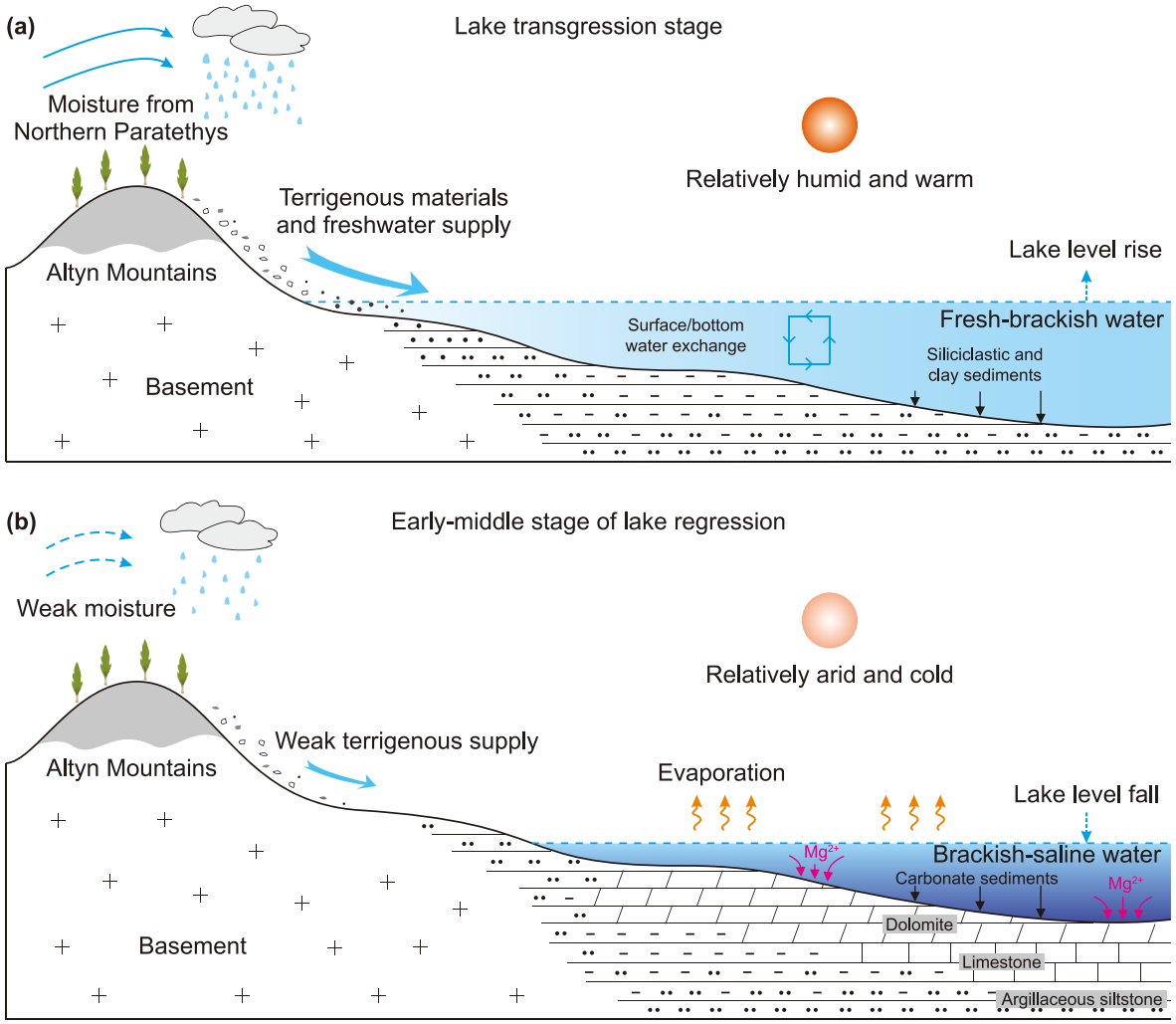


**Fig. 7.** Conceptual model illustrating the evaporation-driven dolomitization during the syngenetic-penecontemporaneous stage within an individual depositional sequence and its control by climate change and lake evolution.

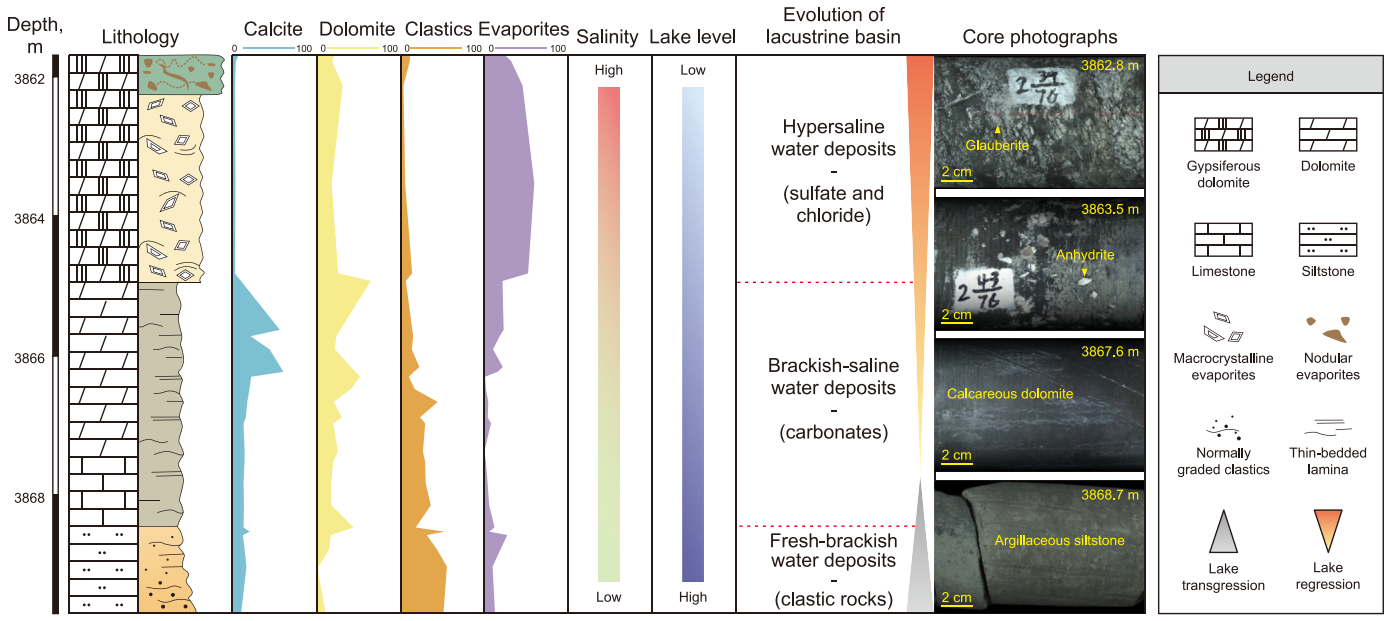


**Fig. 8.** Comprehensive columns of a typical cored interval of Well S41-6-1 showing the variations in lithology and mineralogy and lake evolution associated with an individual dolomitization event.

mixed siliciclastic-carbonate-evaporite deposits in the Eocene Qaidam Basin, with the superposition of multistage relatively short-term dolomitization events and periodic variation in the dolomite abundance in the vertical direction. In addition to the replacive dolomites, microbial dolomite precipitation, indicated by the coincidence of microbial fabrics and Mg-enriched zones observed in an electron probe energy spectrum scan (Huang et al., 2016), occurred occasionally in local paleo-highlands.

In general, the periodic evaporation and resulting salinization processes of the semiclosed lacustrine basin, which are regulated by regional tectonic-climatic changes, were primarily responsible for the early dolomitization. The cyclic and sequential change in mineral paragenesis from terrigenous clastic rocks to carbonates to evaporites gives rise to the vertical heterogeneity in the dolomite abundance since it determines the amount of limestone precursor available for replacive dolomitization. Additionally, the simulation results imply that the infiltration depth of the brine was mainly affected by the duration of the dolomitization (or evaporation) event during regression (Fig. 6a). Given the high-frequency fluctuations of lake level and water salinity during the Eocene (Jiang et al., 2019; Xiong et al., 2021b), the basin was not likely to be dominated by prolonged intense evaporation, and the recharge of the brine (evaporated lake water) into the formation was limited. Hence, the infiltration depth of dolomitizing fluid was likely to have been limited by the frequent water salinity fluctuation and the insufficient brine recharge, which also led to a relatively low degree of dolomitization and low dolomite abundance in the lower part of the sequence (Fig. 8).

### 5.2. Controls on the rate of dolomitization

Through sensitivity analyses of the various lithological and hydrogeochemical parameters, the potential factors controlling dolomitization have been discussed in previous RTM studies (Whitaker and Xiao, 2010; Al-Helal et al., 2012; Yang et al., 2022b). These factors include extrinsic controls, such as platform geometry, temperature, and salinity, chemical composition, and flux of the brine, and intrinsic controls, such as lithofacies, initial porosity and permeability, RSA, and crystal nucleus and lattice defects. Generally, the dolomitization process can be accelerated by higher water salinity, temperature, RSA and fluid injection rate and a higher degree of dolomitization can be achieved under conditions of higher water salinity, temperature and fine-grained rock fabric (Al-Helal et al., 2012; Gabellone and Whitaker, 2016). For the specific geological setting in the study area, we focus on the potential uncertainty in the parameters involved in model construction, including evaporation intensity and dolomite crystal size.

(1) Evaporation intensity (lake water salinity)

The variation in evaporation intensity (lake water salinity) in a lacustrine environment is the result of the combined effects of solar radiation, wind, waves, and geomorphological barriers (Guo et al., 2018; Jiang et al., 2019), which can alter the saturation state of the solution with respect to carbonate/evaporite minerals. The results of the sensitivity analysis of lake water salinity (Fig. 9a–c) show that there is an obvious increasing trend in dolomite precipitation with water salinity. Specifically, with the increase in water salinity from 45.2‰ to 113‰, the amount of dolomite precipitation increases by more than 10 times (at the same depth) and the seepage depth of the dolomitizing fluid increases from 5 m to 8 m (Fig. 9a). At a water salinity of 226‰, dolomitization of the whole column reaches equilibrium in less than 2 kyr in the simulation, while the equilibration time for the base case simulation (salinity of 113‰) is approximately 5 kyr. These results indicate a significantly higher rate of dolomitization and a greater seepage depth of the dolomitizing fluid under stronger evaporation. This is mainly because the increases in water salinity (higher $Mg^{2+}$ and $HCO_3^-$ concentrations) and ion activity product enhance the kinetic reaction rate (Eq. (3)) and thus facilitate dolomite precipitation. Moreover, the density of the brine also increases with the gradual evaporation of water, which helps the dolomitizing fluid permeate into deeper formations, driven by gravity. In addition to promoting dolomite precipitation, a higher water salinity also facilitates gypsum cementation at the dolomite front, as shown by the increase in the gypsum volume from 4.0% to 6.2% with an increase in the water

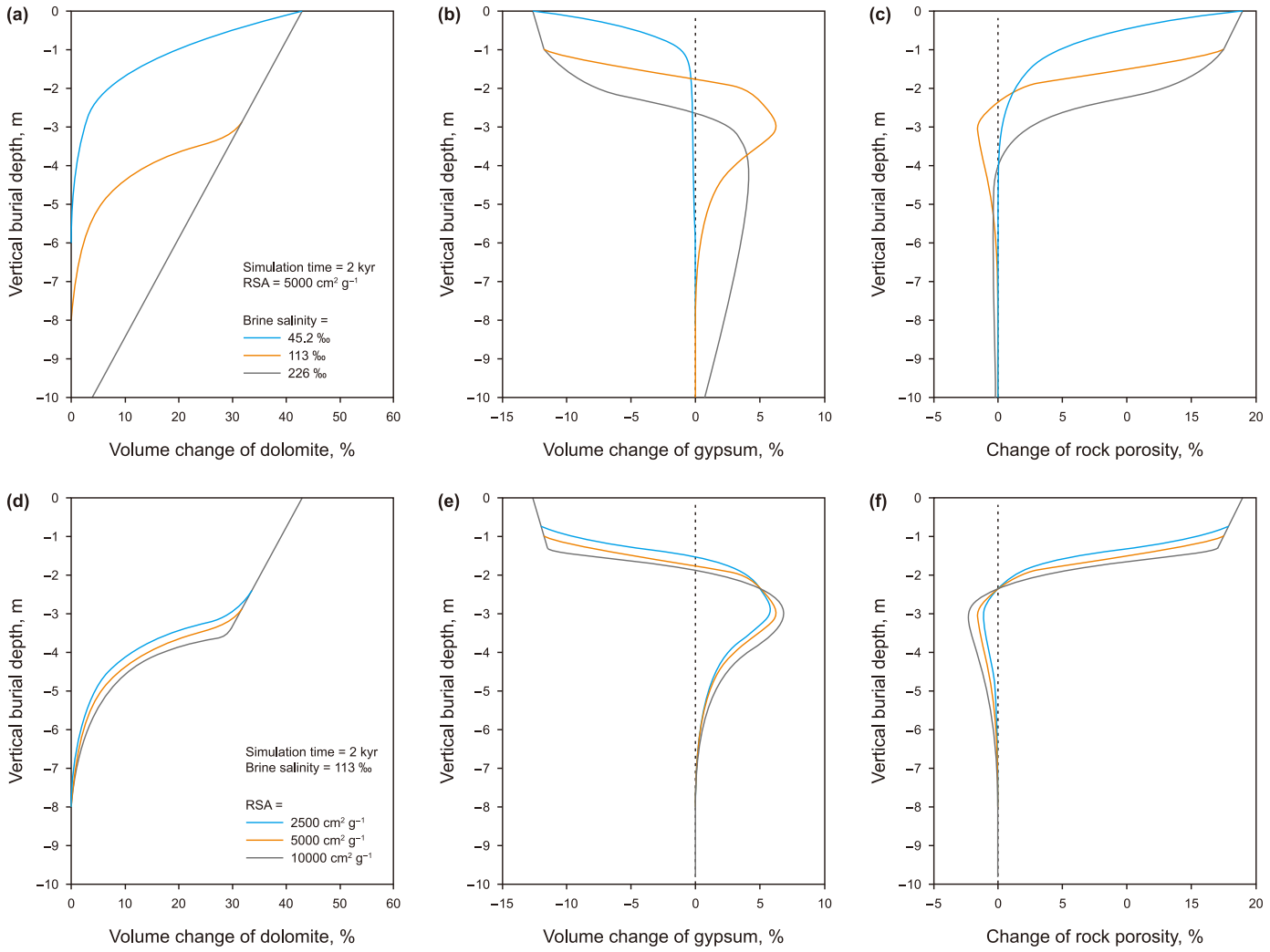


**Fig. 9.** Simulation results of sensitivity analyses showing the impacts of (**a-c**) lake water salinity and (**d-f**) reactive surface area on the mineral and porosity changes during dolomitization.

salinity from 113‰ to 226‰ (Fig. 9b). At a water salinity of 45.2‰, gypsum cementation was not observed, probably due to the relatively low $SO_4^{2-}$ concentration in the injected solution.

Our results are comparable to previous simulations of 1D or 2D generic models using several types of brine from modern environments (e.g., concentrated modern seawater, Aptian seawater, Mississippian seawater) as dolomitizing fluids (Jones and Xiao, 2005; Gabellone and Whitaker, 2016; Lu and Cantrell, 2016), which highlight the significant impact of evaporation intensity on the enhancements of dolomite supersaturation and density-driven fluid flux during dolomitization. Notably, Gabellone and Whitaker (2016) recorded apparent precipitation of dolomite cements (overdolomitization) and resulting porosity decline proximal to the brine source after complete replacement of calcite. However, this overdolomitization process was not observed in our simulation. This might be attributed to the relatively low temperature (26.2 °C) and short simulation time (5 kyr) of our study since a high dolomitizing fluid flux, high temperature, and long time period (several million years) are generally considered to be necessary for overdolomitization (Machel, 2004; Whitaker et al., 2004; Al-Helal et al., 2012).

(2) Particle size (reactive surface area)

The RSA is often used to describe the reactivity of porous sediments and is regarded as an important rate-determining factor of water-rock interaction (German and Park, 2009; Beckingham et al., 2016). The results of the sensitivity analysis of RSA (Fig. 9d–f) show that before equilibrium both the dolomite precipitation and gypsum cementation were enhanced slightly with increasing RSA. This indicates that the higher reactivity of fine-grained sediments than coarse-grained sediments leads to a relatively higher rate of dolomitization. Nevertheless, the promotion effect for dolomite precipitation and gypsum cementation resulting from increasing RSA is much less significant than that resulting from an increase in water salinity (Fig. 10a), as evidenced by the minor variations in the dolomite content (from 11.7% to 16.4% at the depth of −4 m after 2 kyr of simulation) and gypsum content (from 6.8% to 7.3% at the dolomite front) even with a massive change in the RSA from 2500 $cm^2\ g^{-1}$ to 10,000 $cm^2\ g^{-1}$. Therefore, the evaporation intensity associated with the different depositional sequences should be the major rate-determining factor of the dolomitization process in the Eocene Qaidam Basin.

The influence of RSA on water-rock interactions is commonly assessed in combination with fluid mobility in porous sediments, as the RSA is the major rate-determining factor in permeable systems while the fluid mobility is the major rate-determining factor in

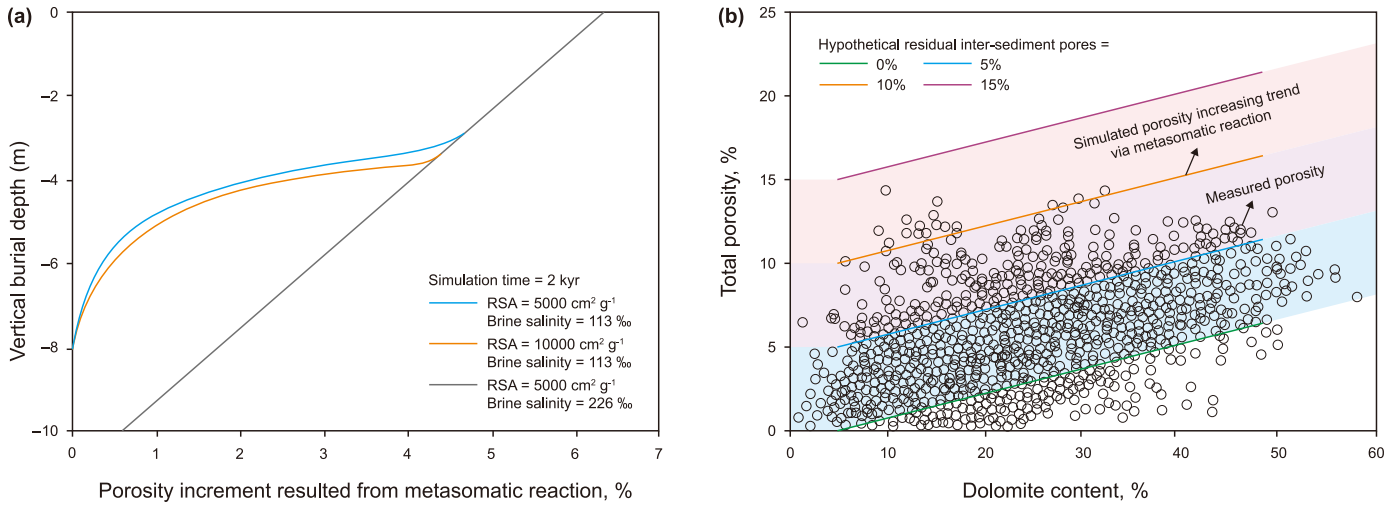


**Fig. 10.** Comparative analysis of the simulated rock porosity evolution and measured reservoir physical property data. (**a**) Simulated rock porosity increase resulting from the metasomatic reaction under different brine salinity and reactive surface area conditions. (**b**) Overlap of the simulated increasing porosity trend during dolomitization (solid lines) with the measured dolomite content vs. porosity scatter plot (circles).

impermeable systems (Harrison et al., 2017; Budd and Park, 2018). In comparison with previous RTM studies in which clear rapid dolomitization was observed with increasing RSA (Jones and Xiao, 2005; Al-Helal et al., 2012), the relatively low initial porosity and permeability values in our model are likely to be the limiting factor of fluid mobility that leads to the minor influence of the RSA on the dolomitization rate.

### 5.3. Formation mechanism of dolomite reservoirs

#### 5.3.1. Correlation between dolomitization and reservoir pores

The correlation between dolomitization and dolomite reservoir development has been long discussed, with a major debate regarding whether dolomitization directly produces pores (Ehrenberg et al., 2006; Jiang et al., 2016; Lai et al., 2020). Despite the fact that magnesium is smaller in ionic radius than calcium, comparisons of actual dolomite reservoirs with their limestone precursors have shown that all three different reservoir property outcomes, i.e., increased-porosity, decreased-porosity, and unchanged-porosity dolomitization models, are possible (Dawans and Swart, 1988; Zhang et al., 2010; Yang et al., 2022a). Furthermore, the magnitude of porosity changes remains poorly understood. These uncertainties have introduced difficulties into understanding the precise relationship between dolomitization and reservoir pore evolution. Herein, an integration of simulation results and observational/measured data provides a potential clue in reconstructing the pore evolution during dolomitization in a specific geological setting.

According to the general reaction formula of dolomitization proposed by Morrow (1982), which takes into consideration the different ionic participation due to different hydrogeological environments, the replacement of calcite by dolomite can be expressed as follows:

$$(2-x)CaCO_3 + Mg^{2+} + xCO_3^{2-} \rightarrow CaMg(CO_3)_2 + (1-x)Ca^{2+} \quad (4)$$

where $x$ denotes the stoichiometric number of $CO_3^{2-}$ (ranging 0–1), and the reaction's effect on porosity can be determined based on the disparity in molar volume between dolomite and calcite. Specifically, Chen et al. (1985) and Zhang et al. (2010) calculated the possible porosity change outcomes and proposed three special cases as summarized in Table 4, corresponding to the different hydrogeological systems and inflow/outflow of chemical ions ($Mg^{2+}$, $Ca^{2+}$, and $CO_3^{2-}$) during dolomitization.

In our simulation, the maximum porosity increase resulting from the metasomatic reaction is 6.4% (Fig. 10a; porosity changes caused by gypsum cementation/dissolution are not included), which is lower than the estimated 12.96% porosity increase for an ideal mole-for-mole dolomitization model (Table 4; $x = 0$; 1 mol $Ca^{2+}$ replaced by 1 mol $Mg^{2+}$). This difference likely exists because the initial limestone sediments were not fully dolomitized under the low-temperature conditions in the study area. An alternative interpretation could be that a small quantity of exogenous $CO_3^{2-}$ (or $HCO_3^-$; $x < 0.26$ as indicated in Table 4) from injected brine (evaporated lake water) might have been involved in the replacive reaction (Eq. (4)). This interpretation conforms to the semiclosed saline lacustrine environment in this region, as demonstrated by a prior paleoenvironmental reconstruction (Guo et al., 2018; Xiong et al., 2021b). The precipitation of gypsum at the dolomite front zone during the simulation (Fig. 6c) indicates that some of the $Ca^{2+}$ released by the replacive reaction can be carried away along the flow pathway, which also rules out the possibility of a completely closed hydrogeochemical environment.

Although the porosity changes during dolomitization can be estimated theoretically based on the difference in ionic radius between magnesium and calcium under variable hydrogeological environments, it should be noted that the above evaluation may not be able to fully explain the actual contribution of dolomitization to reservoir pores. A so-called protodolomite-to-dolomite transformation process, which has been recently revealed by dry-heating experiments (Zheng et al., 2021), might also result in additional pores (nanoscopic cavity structures) in dolomite compared to its limestone precursor. The protodolomite, also known as "disordered dolomite" and "very high-magnesian calcite", is a typical metastable predecessor of dolomite (Zheng et al., 2021) and can be both biogenic (via biomineralization) and abiogenic (Sibley et al., 1994; Kaczmarek and Thornton, 2017). Notably, protodolomite has a similar chemical composition (>36 mol% $MgCO_3$) to dolomite, but its lattice structure is disordered (Graf and Goldsmith, 1956). Due to the Mg-hydration effect, protodolomite usually contains structural water (1.4–7%; Zheng et al., 2021), and the water content decreases with increasing

**Table 4**
The three special cases of replacive reaction during dolomitization (derived from Chen et al., 1985).

| Hydrogeological system | Amount of exogenous $CO_3^{2-}$ | Inflow/outflow of $Mg^{2+}$ and $Ca^{2+}$ | Reaction formula | Theoretical porosity change |
|---|---|---|---|---|
| completely closed environment | $x = 0$ | $Mg^{2+}$ inflow equals $Ca^{2+}$ outflow | $2CaCO_3 + Mg^{2+} \rightarrow CaMg(CO_3)_2 + Ca^{2+}$ | Increase of 12.96% |
| Semiclosed environment | $x = 0.26$ | $Mg^{2+}$ inflow greater than $Ca^{2+}$ outflow | $1.74CaCO_3 + Mg^{2+} + 0.26CO_3^{2-} \rightarrow CaMg(CO_3)_2 + 0.74Ca^{2+}$ | Unchanged |
| Open environment | $x = 1$ | No $Ca^{2+}$ outflow | $CaCO_3 + Mg^{2+} + CO_3^{2-} \rightarrow CaMg(CO_3)_2$ | Decrease of 74.07% |

synthesis temperature. With the rise in temperature during burial, this high-Mg calcite or disordered dolomite tends to gradually transform into ordered dolomite, accompanied by the release of the structural water (dehydration) from the protodolomite. Meanwhile, transformation of the dolomite crystal morphology has also been observed by Zheng et al. (2021), from nanoscopic globular subunits (amorphous solid) to submicron-scale rhombohedral crystalline minerals. Accordingly, a few nanoscopic pores form on the surface or between dolomite crystals. In addition, the released structural water might trigger further dissolution of dolomite and expansion of intercrystalline micropores.

In terms of the Eocene lacustrine dolomite in the western Qaidam Basin, the petrographic and mineralogical evidence from our samples and earlier work (Yuan et al., 2015; Huang et al., 2016) suggest a dominant replacive genesis during the syngenetic-penecontemporaneous stage with microbial mediation in local areas. Given the very low mean global temperature (~10 °C) in the Eocene (Miller et al., 2020), these early metastable dolomites, which include microbial mineralization-associated very high-Mg calcite and disordered dolomite formed via very early dolomitization, might have contained some structural water because a low synthesis temperature and biogenesis of dolomite are generally thought to result in higher contents of structural water in dolomite lattices (Xu et al., 2013; Zheng et al., 2021). The presence of structural water provides the foundation for subsequent dehydration and formation of pervasive intercrystalline micropores in dolomite during burial. Specifically, microscopic observation (FSEM) shows that the microcrystalline dolomites in the study area have euhedral submicron-scale rhombohedral crystal structures (Fig. 4g), which is very similar to the products (ordered dolomite) of the dry-heating experiments of protodolomite conducted by Zheng et al. (2021). Furthermore, the strong evaporation and resulting hypersaline brine-dominated pore fluid environment during early diagenesis (near-surface to shallow burial) were conducive to the conversion of early metastable dolomite into ordered dolomite (Oomori et al., 1983; Schmidt et al., 2005), forming euhedral rhombohedral crystals. The above observations indicate that the transformation of the lattice structure and associated dehydration process are likely to have taken place in the formation of the ordered dolomites in the study area. This also explains why the microcrystalline dolomites in the Eocene strata of the Qaidam Basin have good porosities (Fig. 4h; widespread submicron-scale intercrystalline micropores) and constitute a unique type of tight carbonate reservoir, while the microcrystalline dolomites in other basins (Tarim and Ordos Basins, etc.; Jiang et al., 2018; Xiao et al., 2021) generally have poor reservoir capacities. The disordered irregular structures of the dolomite crystals and the lack of continuous evaporation and a brine-dominated pore fluid environment during burial indicate that the microcrystalline dolomites in other basins might not have experienced the dehydration process. Moreover, the nanoscopic dissolution characteristics of some dolomite crystals in the study area (Fig. 4i) can thus be interpreted as relating to the slight dissolution induced by the release of structural water during transformation of disordered to ordered dolomites.

### 5.3.2. Contributions of different porosity generation mechanisms

By comparing simulation results with measured mineralogical data and physical properties of the dolomite reservoirs, the relative importance of different porosity generation mechanisms can also be assessed. First, the numerical simulations (Fig. 6) documented an increasing trend in porosity with dolomitization and the simulated dolomite content ranges from 5.0% to 48.1%, which is comparable to the dolomite abundance measured by the whole-rock XRD tests. However, the maximum porosity increase via dolomitization is 6.4% in the simulations (Fig. 10a), which is lower than the measured dolomite porosity (up to 15%; circles in Fig. 10b), indicating that additional or alternative porosity generation mechanisms were likely involved in the formation of the dolomite reservoirs in the study area. As discussed in previous studies, the Eocene dolomite reservoirs in the western Qaidam Basin are the products of multiple pore-increasing/decreasing effects, potentially including the preservation of original intergranular pores, pore reduction due to compaction, and pore increases via dolomitization, near-surface or burial dissolution, and formation of microfractures during late diagenesis (Huang et al., 2016; Liu et al., 2017). Specifically, given the complex formation pressure system and disequilibrium of compaction during burial (e.g., the presence of local abnormal overpressure) caused by the rapid deposition, sealing by gypsum/halite-salt rock, and conversion and dehydration of gypsum (Guo et al., 2019; Li et al., 2021), the amount of residual intergranular pores inherited from the parent sediments after compaction is of high uncertainty. Therefore, four different hypothetical residual porosities, i.e., 0%, 5%, 10%, and 15% (solid lines in Fig. 10b), were considered in simulation results for parametric uncertainty analysis, representing an increase in the degree of preservation of original intergranular pores. An overlap of the simulated increasing porosity trend during dolomitization with the measured dolomite content vs. porosity scatter plot (Fig. 10b) indicates that the residual intergranular porosity after compaction mostly ranges from 0 to 10%, and that the dolomitization gives rise to a porosity increment of 0–8%. Moreover, a few samples yield low dolomite contents but relatively high porosity, which can be attributed to the result of slight karstification or fracture porosity (Huang et al., 2017; Xiong et al., 2021b).

In general, the integrated RTM simulations and rock mineralogical and physical property measurements suggest that the preservation of original intergranular pores and the subsequent porosity generation via early dolomitization are the major mechanisms contributing to the unique microcrystalline dolomite reservoirs in the western Qaidam Basin. The ability to quantitatively evaluate the contributions of various porosity generation mechanisms highlights the promising prospect of this integrated approach in applications to carbonate reservoirs elsewhere with multiple and complex geneses.

### 5.4. Significance and limitations

RTM constraints on dolomite formation have been implemented in various depositional and burial environments, such as marine carbonate platform (Lu and Cantrell, 2016), platform margin (Al-Helal et al., 2012), epeiric ramp (Gabellone et al., 2016) and burial fracture systems (Wei et al., 2017). The present study further expands the application of RTM for dolomite problems to evaporative lacustrine environments. Our results, together with previous RTM work, is of sedimentological and hydrocarbon significance for understanding the hydrogeochemical mechanisms of dolomitization process in diverse environments and the associated coevolution of fluids, mineralogy and reservoir properties.

Nevertheless, before the dolomite mystery can be fully resolved and the RTM method is regularly applied for realistic reservoir prediction, there are still a few obstacles to overcome. On the one hand, there are still some limitations related to the kinetic model of dolomitization. For instance, the microbial effect is not considered in the current model, although microbial mediation has been regarded as an important factor for promoting the early precipitation of Mg-carbonates (Perri and Tucker, 2007; Dupraz et al., 2009). Additionally, in the current simulations, the dolomitization process is treated as a reaction network that comprises calcite dissolution followed by dolomite precipitation, while whether there is dissolution of calcite in a real replacement process remains controversial. On the other hand, it is still difficult to couple the dolomitization process during the syngenetic-penecontemporaneous stage with the other complex diagenetic processes during a long burial period, which makes it difficult to extend the simulation of dolomite formation to the whole geological history. Thus, the current model cannot fully explain the formation mechanism and evolution of the massive dolomites in ancient strata as it does not consider the recrystallization or neomorphism of early dolomites caused by gradual changes in temperature and pressure during burial.

In further research, thermodynamic/kinetic processes of water-rock interactions in more practical and complex geological settings, such as the microbial-induced dolomite precipitation and the coupling of early reflux dolomitization with burial recrystallization and hydrothermal alteration processes, should be investigated. It is also important to emphasize the integration of traditional geological methods and the RTM approach, particularly the cross-validation of simulation and laboratory findings. These topics are expected to soon draw researchers interested in sedimentology and diagenesis.

## 6. Conclusions

The Eocene western Qaidam Basin was dominated by mixed siliciclastic-carbonate-evaporite sedimentation in a semiclosed saline lacustrine environment. The complexity of the lacustrine mixed deposits makes it difficult to determine the dolomite distribution and reservoir genesis through the use of petrology and geochemistry alone. This issue was addressed by integrated usage of RTM simulation. This method, which is highly useful in hydrogeochemical studies, can be applied to geological issues and shows promising prospects.

Periodic evaporation and salinization processes in the lacustrine basin during syngenetic-penecontemporaneous stage led to the superimposition of multiple short-term dolomitization events. The cyclic variation in dolomite abundance was essentially caused by the successive change in mineral paragenesis from terrigenous clastics to carbonates to evaporites, which determined the amount of limestone precursor available for replacive dolomitization. The evaporation intensity and particle size of sediments were rate-determining factors of the dolomitization process. The preservation of original intergranular pores and generation of porosity via early dolomitization were the major formation mechanisms of the distinctive microcrystalline dolomite reservoirs.

Given that the natural geological systems are more complex than numerical models which always require necessary simplification and assumptions, our results also have limitations, particularly in extrapolating the fluid-mineral-porosity evolution to the whole geological history since the current model lacks the consideration of sedimentary heterogeneity and burial diagenetic alteration. Nevertheless, the reconstruction of dolomitizing fluid-rock interactions, based on the thermo-hydro-chemical coupled modeling, provides a better understanding of the hydrogeochemical mechanism of dolomitization process and can help to reduce uncertainty of dolomite reservoir prediction in the complex lacustrine environment.

## CRediT authorship contribution statement

**Ying Xiong:** Conceptualization, Data curation, Writing – original draft. **Bo Liu:** Supervision. **Xiu-Cheng Tan:** Supervision. **Zheng-Meng Hou:** Supervision, Writing – review & editing. **Jia-Shun Luo:** Software. **Ya-Chen Xie:** Software. **Kai-Bo Shi:** Investigation. **Kun-Yu Wu:** Data curation.

## Declaration of competing interest

The authors declare that they have no known competing financial interests or personal relationships that could have appeared to influence the work reported in this paper.

## Acknowledgments

We appreciate two anonymous reviewers for the constructive comments in improving the manuscript.

## Appendix A. Supplementary data

Supplementary data to this article can be found online at https://doi.org/10.1016/j.petsci.2024.03.008.

## References

Abels, H.A., Dupont-Nivet, G., Xiao, G., Bosboom, R., Krijgsman, W., 2011. Step-wise change of asian interior climate preceding the eocene–oligocene transition (EOT). Palaeogeogr. Palaeoclimatol. Palaeoecol. 299, 399–412. https://doi.org/10.1016/j.palaeo.2010.11.028.

Al-Helal, A., Whitaker, F., Xiao, Y.T., 2012. Reactive transport modeling of brine reflux: dolomitization, anhydrite precipitation, and porosity evolution. J. Sediment. Res. 82, 196–215. https://doi.org/10.2110/jsr.2012.14.

An, Z.S., Kutzbach, J.E., Prell, W.L., Porter, S.C., 2001. Evolution of Asian monsoons and phased uplift of the Himalaya-Tibetan plateau since Late Miocene times. Nature 411, 62–66. https://doi.org/10.1038/35075035.

Arvidson, R.S., Mackenzie, F.T., 1999. The dolomite problem; control of precipitation kinetics by temperature and saturation state. Am. J. Sci. 299, 257–288. https://doi.org/10.2475/ajs.299.4.257.

Bao, J., Wang, Y.D., Song, C.H., Feng, Y., Hu, C.H., Zhong, S.R., Yang, J.W., 2017. Cenozoic sediment flux in the Qaidam Basin, northern Tibetan Plateau, and implications with regional tectonics and climate. Global Planet. Change 155, 56–69. https://doi.org/10.1016/j.gloplacha.2017.03.006.

Beckingham, L.E., Mitnick, E.H., Steefel, C.I., Zhang, S., Voltolini, M., Swift, A.M., Yang, L., Cole, J.M., Ajo-Franklin, J.B., DePaolo, A.J., Mito, S., Xue, Z.Q., 2016. Evaluation of mineral reactive surface area estimates for prediction of reactivity of a multi-mineral sediment. Geochem. Cosmochim. Acta 188, 310–329. https://doi.org/10.1016/j.gca.2016.05.040.

Bian, Q., Zhang, D.W., Yu, X.J., Cheng, X., Du, W., Liu, R.C., Wang, Z.D., Guo, Z.J., 2019. Transpressional salt tectonic system in western Qaidam Basin, Western China. AAPG Bull. 103, 547–568. https://doi.org/10.1306/08161817119.

Bosboom, R.E., Abels, H.A., Hoorn, C., van den Berg, B.C., Guo, Z., Dupont-Nivet, G., 2014. Aridification in continental Asia after the middle Eocene climatic optimum (MECO). Earth Planet Sci. Lett. 389, 34–42. https://doi.org/10.1016/j.epsl.2013.12.014.

Budd, D.A., Park, A.J., 2018. Formation of bed-scale spatial patterns in dolomite

abundance during early dolomitization: Part I. Mechanisms and feedbacks revealed by reaction-transport modelling. Sedimentology 65, 209–234. https://doi.org/10.1111/sed.12400.
Chen, Y.H., Liu, Y., Sun, T., 1985. Change of pore volume in dolomitization. Exp. Pet. Geol. 7, 29–37. https://doi.org/10.11781/sysydz198501029 (in Chinese).
Dawans, J.M., Swart, P.K., 1988. Textural and geochemical alternations in Late Cenozoic Bahamian dolomites. Sedimentology 35 (3), 385–403. https://doi.org/10.1111/j.1365-3091.1988.tb00993.x.
Deng, H., Gharasoo, M., Zhang, L.W., Dai, Z.X., Hajizadeh, A., Peters, C., Soulaine, C., Thullner, M., Van Cappellen, P., 2022. A perspective on applied geochemistry in porous media: reactive transport modeling of geochemical dynamics and the interplay with flow phenomena and physical alteration. Appl. Geochem. 146, 105445. https://doi.org/10.1016/j.apgeochem.2022.105445.
Dupraz, C., Reid, R.P., Braissant, O., Decho, A.W., Norman, R.S., Visscher, P.T., 2009. Processes of carbonate precipitation in modern microbial mats. Earth Sci. Rev. 96, 141–162. https://doi.org/10.1016/j.earscirev.2008.10.005.
Ehrenberg, S.N., Eberli, G.P., Keramati, M., Moallemi, S.A., 2006. Porosity-permeability relationships in interlayered limestone-dolostone reservoirs. AAPG Bull. 90, 91–114. https://doi.org/10.1306/08100505087.
Fang, X.M., Zhang, W.L., Meng, Q.Q., Gao, J.P., Wang, X.M., King, J., Song, C.H., Dai, S., Miao, Y.F., 2007. High-resolution magnetostratigraphy of the neogene huaitoutala section in the eastern Qaidam Basin on the NE Tibetan plateau, Qinghai province, China and its implication on tectonic uplift of the NE Tibetan plateau. Earth Planet Sci. Lett. 258, 293–306. https://doi.org/10.1016/j.epsl.2007.03.042.
Feng, Z.Z., Zhang, Y.S., Jin, Z.K., 1998. Type, origin, and reservoir characteristics of dolostones of the ordovician majiagou group, Ordos, north China platform. Sediment. Geol. 118, 127–140. https://doi.org/10.1016/S0037-0738(98)00009-8.
Gabellone, T., Whitaker, F., 2016. Secular variations in seawater chemistry controlling dolomitization in shallow reflux systems: insights from reactive transport modelling. Sedimentology 63 (5), 1233–1259. https://doi.org/10.1111/sed.12259.
Gabellone, T., Whitaker, F., Katz, D., Griffiths, G., Sonnenfeld, M., 2016. Controls on reflux dolomitisation of epeiric-scale ramps: insights from reactive transport simulations of the Mississippian Madison Formation (Montana and Wyoming). Sediment. Geol. 345, 85–102. https://doi.org/10.1016/j.sedgeo.2016.09.003.
Garcia-Fresca, B., Lucia, F.J., Sharp, J.M., Kerans, C., 2012. Outcrop-constrained hydrogeological simulations of brine reflux and early dolomitization of the permian san andres FormationHydrogeologic model of reflux dolomitization of the san andres formation. AAPG Bull. 96, 1757–1781. https://doi.org/10.1306/02071210123.
German, R.M., Park, S.J., 2009. Handbook of Mathematical Relations in Particulate Materials Processing: Ceramics, Powder Metals, Cermets, Carbides, Hard Materials, and Minerals, vol. 3. John Wiley & Sons. https://doi.org/10.1002/9780470370087.
Graf, D.L., Goldsmith, J.R., 1956. Some hydrothermal syntheses of dolomite and protodolomite. J. Geol. 64 (2), 173–186. https://doi.org/10.1086/626332.
Guo, P., Liu, C.Y., Huang, L., Wang, P., Wang, K., Yuan, H.L., Xu, Z.K., Zhang, Y.Y., 2017. Genesis of the late Eocene bedded halite in the Qaidam Basin and its implication for paleoclimate in East Asia. Paleogeogr. Paleoclimatol. Paleoecol. 487, 364–380. https://doi.org/10.1016/j.palaeo.2017.09.023.
Guo, P., Liu, C.Y., Huang, L., Yu, M.L., Wang, P., Zhang, G.Q., 2018. Palaeohydrological evolution of the late Cenozoic saline lake in the Qaidam Basin, NE Tibetan Plateau: tectonic vs. climatic control. Global Planet. Change 165, 44–61. https://doi.org/10.1016/j.gloplacha.2018.03.012.
Guo, R.T., Ma, D.D., Zhang, Y.S., Liu, B., Chen, X.D., Cui, J., Wang, P., Zhang, Q.H., Jiang, Y.H., Li, Y.F., 2019. Characteristics and formation mechanism of overpressure pore-fracture reservoirs for upper member of Xiaganchaigou Formation in the west of yingxiong ridge, Qaidam Basin. Acta Pet. Sin. 40 (4), 411–422. https://doi.org/10.7623/syxb201904003 (in Chinese).
Harrison, A.L., Dipple, G.M., Song, W., Power, I.M., Mayer, K.U., Beinlich, A., Sinton, D., 2017. Changes in mineral reactivity driven by pore fluid mobility in partially wetted porous media. Chem. Geol. 463, 1–11. https://doi.org/10.1016/j.chemgeo.2017.05.003.
Huang, C.G., Yuan, J.Y., Cao, Z.L., Zhang, S.M., Wang, Y., She, M., 2015. Simulate experiment study about the saline fluid-rock interaction in the clastic reservoir of the saline lacustrine basin. Bull. China Soc. Mineral Petrol. Geochem. 34 (2), 343–348. https://doi.org/10.3969/j.issn.1007-2802.2015.02.016 (in Chinese).
Huang, C.G., Yuan, J.Y., Tian, G.R., Wu, L.R., Pan, X., Hui, Y.Y., 2016. The geochemical characteristics and formation mechanism of the Eocene lacustrine dolomite reservoirs in the western Qaidam. Earth Sci. Front. 23 (3), 230–242. https://doi.org/10.13745/j.esf.2016.03.027 (in Chinese).
Huang, C.G., Guan, X., Ni, X.L., Chang, H.Y., Zhang, S.M., Yang, S., 2017. The characteristics and major factors controlling on the $E_3^2$ dolomite reservoirs in saline lacustrine basin in the Yingxi area of Qaidam Basin. Nat. Gas Geosci. 28 (2), 219–231. https://doi.org/10.11764/j.issn.1672-1926.2016.12.005 (in Chinese).
Jiang, L., Cai, C.F., Worden, R.H., Crowley, S.F., Jia, L.Q., Zhang, K., Duncan, I.J., 2016. Multiphase dolomitization of deeply buried Cambrian petroleum reservoirs, Tarim Basin, north-west China. Sedimentology 63, 2130–2157. https://doi.org/10.1111/sed.12300.
Jiang, L., Worden, R.H., Cai, C.F., Shen, A.J., Crowley, S.F., 2018. Diagenesis of an evaporite-related carbonate reservoir in deeply buried Cambrian strata, Tarim Basin, Northwest China. AAPG Bull. 102 (1), 77–102. https://doi.org/10.1306/0328171608517048.
Jiang, Q.C., Ma, Y.S., Shen, Y.C., Guo, R.T., Gao, X.Q., Liu, B., Cui, J., Wu, K.Y., 2019. High-frequency redox variations of the Eocene cyclic lacustrine sediments in the Yingxi area, western Qaidam Basin, China. J. Asian Earth Sci. 174, 135–151. https://doi.org/10.1016/j.jseaes.2018.11.025.
Jolivet, M., Brunel, M., Seward, D., Xu, Z., Yang, J., Roger, F., Tapponnier, P., Malavieille, J., Arnaud, N., Wu, C., 2001. Mesozoic and Cenozoic tectonics of the northern edge of the Tibetan plateau: fission-track constraints. Tectonophysics 343, 111–134. https://doi.org/10.1016/S0040-1951(01)00196-2.
Jones, G.D., Xiao, Y.T., 2005. Dolomitization, anhydrite cementation, and porosity evolution in a reflux system: insights from reactive transport models. AAPG Bull. 89, 577–601. https://doi.org/10.1306/12010404078.
Kaczmarek, S.E., Thornton, B.P., 2017. The effect of temperature on stoichiometry, cation ordering, and reaction rate in high-temperature dolomitization experiments. Chem. Geol. 468, 32–41. https://doi.org/10.1016/j.chemgeo.2017.08.004.
Kaufmann, G., 2016. Modelling karst aquifer evolution in fractured, porous rocks. J. Hydrol. 543, 796–807. https://doi.org/10.1016/j.jhydrol.2016.10.049.
Lai, J., Wang, S., Zhang, C.S., Wang, G.W., Song, Q.Q., Chen, X., Yang, K.F., Yuan, C.J., 2020. Spectrum of pore types and networks in the deep cambrian to lower ordovician dolostones in tarim basin, China. Mar. Petrol. Geol. 112, 104081. https://doi.org/10.1016/j.marpetgeo.2019.104081.
Lasaga, A.C., Soler, J.M., Ganor, J., Burch, T.E., Nagy, K.L., 1994. Chemical weathering rate laws and global geochemical cycles. Geochem. Cosmochim. Acta 58, 2361–2386. https://doi.org/10.1016/0016-7037(94)90016-7.
Last, W.M., 1990. Lacustrine dolomite—an overview of modern, Holocene, and Pleistocene occurrences. Earth Sci. Rev. 27 (3), 221–263. https://doi.org/10.1016/0012-8252(90)90004-F.
Li, P., Liu, C.L., Feng, D.H., Tai, W.X., Tian, J.X., Yang, T.Z., Ran, Y., 2021. Characteristics and origin mechanism of formation overpressure in the saline lacustrine basin: a case study from the Oligocene in the west of Yingxiong ridge, Qaidam Basin. J. China Univ. Min. Technol. 50, 864–876. https://doi.org/10.13247/j.cnki.jcumt.001269 (in Chinese).
Li, Q., Zhang, Y., Dong, L., Guo, Z., 2018. Oligocene syndepositional lacustrine dolomite: a study from the southern Junggar Basin, NW China. Paleogeogr. Paleoclimatol. Paleoecol. 503, 69–80. https://doi.org/10.1016/j.palaeo.2018.04.004.
Liu, Z.G., Zhu, C., Li, S.M., Xue, J.Q., Gong, Q.S., Wang, Y.Q., Wang, P., Xia, Z.Y., Song, G.Y., 2017. Geological features and exploration fields of tight oil in the Cenozoic of western Qaidam Basin, NW China. Petrol. Explor. Dev. 44, 196–204. https://doi.org/10.1016/S1876-3804(17)30024-1.
Lu, P., Cantrell, D., 2016. Reactive transport modelling of reflux dolomitization in the Arab-D reservoir, Ghawar field, Saudi Arabia. Sedimentology 63, 865–892. https://doi.org/10.1111/sed.12241.
Lucia, F.J., 1995. Rock-fabric/petrophysical classification of carbonate pore space for reservoir characterization. AAPG Bull. 79, 1275–1300. https://doi.org/10.1306/7834D4A4-1721-11D7-8645000102C1865D.
Machel, H.G., 2004. Concepts and models of dolomitization: a critical reappraisal. Geol. Soc. London, Spec. Publ. 235 (1), 7–63. https://doi.org/10.1144/GSL.SP.2004.235.01.02.
Miller, K.G., Browning, J.V., Schmelz, W.J., Kopp, R.E., Mountain, G.S., Wright, J.D., 2020. Cenozoic sea-level and cryospheric evolution from deep-sea geochemical and continental margin records. Sci. Adv. 6. https://doi.org/10.1126/sciadv.aaz1346 eaaz1346.
Morrow, D.W., 1982. Diagenesis 1. dolomite - part 1: the chemistry of dolomitization and dolomite precipitation. Geosci. Can. 9, 5–13. https://id.erudit.org/iderudit/geocan9_1art02.
Oomori, T., Kaneshima, K., Taira, T., Kitano, Y., 1983. Synthetic studies of protodolomite from brine waters. Geochem. J. 17 (3), 147–152. https://doi.org/10.2343/geochemj.17.147.
Parkhurst, D.L., Appelo, C.A.J., 1999. User's guide to PHREEQC (Version 2): a computer program for speciation, batch-reaction, one-dimensional transport, and inverse geochemical calculations. Water-Resour. Invest. Rep. 99 (4259), 312. https://doi.org/10.3133/wri994259.
Perri, E., Tucker, M., 2007. Bacterial fossils and microbial dolomite in Triassic stromatolites. Geology 35, 207–210. https://doi.org/10.1130/G23354A.1.
Schmidt, M., Xeflide, S., Botz, R., Mann, S., 2005. Oxygen isotope fractionation during synthesis of CaMg-carbonate and implications for sedimentary dolomite formation. Geochem. Cosmochim. Acta 69 (19), 4665–4674. https://doi.org/10.1016/j.gca.2005.06.025.
Sibley, D.F., Nordeng, S.H., Borkowski, M.L., 1994. Dolomitization kinetics of hydrothermal bombs and natural settings. J. Sediment. Res. 64, 630–637. https://doi.org/10.1306/D4267E29-2B26-11D7-8648000102C1865D.
Sobel, E.R., 1999. Basin analysis of the jurassic–lower cretaceous southwest tarim basin, northwest China. Geol. Soc. Am. Bull. 111, 709–724. https://doi.org/10.1130/0016-7606(1999)111<0709:BAOTJL>2.3.CO;2.
Tapponnier, P., Zhiqin, X., Roger, F., Meyer, B., Arnaud, N., Wittlinger, G., Jingsui, Y., 2001. Oblique stepwise rise and growth of the Tibet Plateau. Science 294 (5547), 1671–1677. https://doi.org/10.1126/science.105978.
Wanas, H.A., Sallam, E., 2016. Abiotically-formed, primary dolomite in the mid-Eocene lacustrine succession at Gebel El-Goza El-Hamra, NE Egypt: an approach to the role of smectitic clays. Sediment. Geol. 343, 132–140. https://doi.org/10.1016/j.sedgeo.2016.08.003.
Wang, J.G., Zhang, D.W., Yang, S.Y., Li, X., Shi, Y.J., Cui, J., Zhang, P., Wang, Y.L., Yi, D.H., Chang, H.Y., 2020. Sedimentary characteristics and genesis of the salt lake with the upper member of the Lower Ganchaigou Formation from Yingxi sag, Qaidam basin. Mar. Petrol. Geol. 111, 135–155. https://doi.org/10.1016/j.marpetgeo.2019.08.006.
Warren, J., 2000. Dolomite: occurrence, evolution and economically important

associations. Earth Sci. Rev. 52, 1–81. https://doi.org/10.1016/S0012-8252(00)00022-2.
Wei, W., Chen, D., Qing, H., Qian, Y., 2017. Hydrothermal dissolution of deeply buried cambrian dolomite rocks and porosity generation: integrated with geological studies and reactive transport modeling in the tarim basin, China. Geofluids, 9562507. https://doi.org/10.1155/2017/9562507, 2017.
Whitaker, F.F., Smart, P.L., Jones, G.D., 2004. Dolomitization: from conceptual to numerical models. Geol. Soc. London, Spec. Publ. 235 (1), 99–139. https://doi.org/10.1144/GSL.SP.2004.235.01.05.
Whitaker, F.F., Smart, P.L., 2007. Geochemistry of meteoric diagenesis in carbonate islands of the northern Bahamas: 2. Geochemical modelling and budgeting of diagenesis. Hydrol. Process. 21, 967–982. https://doi.org/10.1002/hyp.6533.
Whitaker, F.F., Xiao, Y., 2010. Reactive transport modeling of early burial dolomitization of carbonate platforms by geothermal convection. AAPG Bull. 94, 889–917. https://doi.org/10.1306/12090909075.
Wolery, T.J., 1992. EQ3/6, a Software Package for Geochemical Modeling of Aqueous Systems: Package Overview and Installation Guide. Lawrence Livermore National Lab. https://doi.org/10.2172/138894. No. UCRL-MA–110662-PT. 1, version 7.0.
Wu, L., Xiao, A.C., Wang, L.Q., Mao, L.G., Wang, L., Dong, Y.P., Xu, B., 2012. EW-trending uplifts along the southern side of the central segment of the Altyn Tagh Fault, NW China: insight into the rising mechanism of the Altyn Mountain during the Cenozoic. Sci. China Earth Sci. 55, 926–939. https://doi.org/10.1007/s11430-012-4402-7.
Xiao, Y.T., Whitaker, F., Xu, T.F., Steefel, C., 2018. Reactive Transport Modeling: Applications in Subsurface Energy and Environmental Problems. John Wiley & Sons, Incorporated. https://doi.org/10.1002/9781119060031.
Xiao, D., Cao, J., Tan, X.C., Xiong, Y., Zhang, D.F., Dong, G.D., Lu, Z.X., 2021. Marine carbonate reservoirs formed in evaporite sequences in sedimentary basins: a review and new model of epeiric basin-scale moldic reservoirs. Earth Sci. Rev. 223, 103860. https://doi.org/10.1016/j.earscirev.2021.103860.
Xiong, Y., Hou, Z.M., Tan, X.C., Luo, J.S., Yue, Y., Wu, K.Y., 2021a. Constraining fluid-rock interactions during eogenetic karst and their impacts on carbonate reservoirs: insights from reactive transport modeling. Appl. Geochem. 131, 105050. https://doi.org/10.1016/j.apgeochem.2021.105050.
Xiong, Y., Tan, X.C., Wu, K.Y., Xu, Q., Liu, Y., Qiao, Y.P., 2021b. Petrogenesis of the Eocene lacustrine evaporites in the western Qaidam Basin: implications for regional tectonic and climate changes. Sediment. Geol. 416, 105867. https://doi.org/10.1016/j.sedgeo.2021.105867.
Xiong, Y., Tan, X.C., Liu, B., Hou, Z.M., Luo, J.S., Wu, L., Lu, F.F., Xiao, D., 2023. On the dissolution paths and formation mechanisms of paleokarst reservoirs: constraints from reactive transport modeling. Mar. Petrol. Geol. 156, 106462. https://doi.org/10.1016/j.marpetgeo.2023.106462.
Xu, J., Yan, C., Zhang, F., Konishi, H., Xu, H., Teng, H.H., 2013. Testing the cation-hydration effect on the crystallization of Ca–Mg–$CO_3$ systems. Proc. Natl. Acad. Sci. U.S.A. 110 (44), 17750–17755. https://doi.org/10.1073/pnas.1307612110.
Xu, T.F., Sonnenthal, E., Spycher, N., Pruess, K., 2004. TOUGHREACT User's Guide: A Simulation Program for Non-isothermal Multiphase Reactive Geochemical Transport in Variable Saturated Geologic Media (No. LBNL-55460). Lawrence Berkeley National Lab.(LBNL), Berkeley, CA (United States). https://doi.org/10.2172/834237.
Xu, T.F., Sonnenthal, E., Spycher, N., Pruess, K., 2006. TOUGHREACT—a simulation program for non-isothermal multiphase reactive geochemical transport in variably saturated geologic media: applications to geothermal injectivity and $CO_2$ geological sequestration. Comput. Geosci. 32, 145–165. https://doi.org/10.1016/j.cageo.2005.06.014.
Yang, L.L., Xu, T.F., Liu, K.Y., Peng, B., Yu, Z.C., Xu, X.M., 2017. Fluid–rock interactions during continuous diagenesis of sandstone reservoirs and their effects on reservoir porosity. Sedimentology 64, 1303–1321. https://doi.org/10.1111/sed.12354.
Yang, L.L., Yu, L.J., Liu, K.Y., Jia, J.H., Zhu, G.Y., Liu, Q., 2022a. Coupled effects of temperature and solution compositions on metasomatic dolomitization: significance and implication for the formation mechanism of carbonate reservoir. J. Hydrol. 604, 127199. https://doi.org/10.1016/j.jhydrol.2021.127199.
Yang, L.L., Zhu, G.Y., Li, X.W., Liu, K.Y., Yu, L.J., Gao, Z.Y., 2022b. Influence of crystal nucleus and lattice defects on dolomite growth: geological implications for carbonate reservoirs. Chem. Geol. 587, 120631. https://doi.org/10.1016/j.chemgeo.2021.120631.
Yang, Y.B., Fang, X.M., Koutsodendris, A., Ye, C.C., Yang, R.S., Zhang, W.L., Liu, X.M., Gao, S.P., 2016. Exploring Quaternary paleolake evolution and climate change in the western Qaidam Basin based on the bulk carbonate geochemistry of lake sediments. Paleogeogr. Paleoclimatol. Paleoecol. 446, 152–161. https://doi.org/10.1016/j.palaeo.2016.01.021.
Ye, C.C., Yang, Y.B., Fang, X.M., Zhang, W.L., 2016. Late Eocene clay boron-derived paleosalinity in the Qaidam Basin and its implications for regional tectonics and climate. Sediment. Geol. 346, 49–59. https://doi.org/10.1016/j.sedgeo.2016.10.006.
Ye, C.C., Yang, Y.B., Fang, X.M., Zhang, W.L., Song, C.H., Yang, R.S., 2020. Paleolake salinity evolution in the Qaidam Basin (NE Tibetan plateau) between ~42 and 29 ma: links to global cooling and paratethys sea incursions. Sediment. Geol. 409, 105778. https://doi.org/10.1016/j.sedgeo.2020.105778.
Yin, A., Rumelhart, P.E., Butler, R., Cowgill, E., Harrison, T.M., Foster, D.A., Ingersoll, R.V., Zhang, Q., Zhou, X.Q., Wang, X.F., Hanson, A., Raza, A., 2002. Tectonic history of the Altyn Tagh fault system in northern Tibet inferred from Cenozoic sedimentation. Geol. Soc. Am. Bull. 114, 1257–1295. https://doi.org/10.1130/0016-7606(2002)114.
Yuan, J.Y., Huang, C.G., Zhao, F., Pan, X., 2015. Carbon and oxygen isotopic compositions, and palaeoenvironmental significance of saline lacustrine dolomite from the Qaidam Basin, Western China. J. Pet. Sci. Eng. 135, 596–607. https://doi.org/10.1016/j.petrol.2015.10.024.
Zhang, X.F., Liu, B., Cai, Z.X., Hu, W.X., 2010. Dolomitization and carbonate reservoir formation. Geol. Sci. Technol. Inf. 29, 79–85. https://doi.org/10.3969/j.issn.1000-7849.2010.03.012 (in Chinese).
Zheng, W.L., Liu, D., Yang, S.S., Fan, Q.G., Papineau, D., Wang, H.M., Qiu, X., Chang, B., She, Z.B., 2021. Transformation of protodolomite to dolomite proceeds under dry-heating conditions. Earth Planet Sci. Lett. 576, 117249. https://doi.org/10.1016/j.epsl.2021.117249.